



LUND
UNIVERSITY



TRAFFIC INDUCED VIBRATIONS AT ROAD-BRIDGE - Experimental and Numerical Analysis

OSKAR BAGGENS

Structural
Mechanics

Master's Dissertation

Department of Construction Sciences
Structural Mechanics

ISRN LUTVDG/TVSM--12/5184--SE (1-79)

ISSN 0281-6679

TRAFFIC INDUCED VIBRATIONS AT ROAD-BRIDGE - Experimental and Numerical Analysis

Master's Dissertation by
OSKAR BAGGENS

Supervisors:

Nils Rydén *PhD,*

Div. of Engineering Geology, LTH, Lund

Brian Norsk Jensen *MSc,*

MAXLAB, Lund

Examiner:

Kent Persson *PhD,*

Dept. of Construction Sciences, LTH, Lund

Copyright © 2012 by Structural Mechanics, LTH, Sweden.
Printed by Media-Tryck LU, Lund, Sweden, November, 2012 (*Pf*).

For information, address:

Division of Structural Mechanics, LTH, Lund University, Box 118, SE-221 00 Lund, Sweden.

Homepage: <http://www.byggmek.lth.se>

Preface

This master thesis was done as a degree project for my exam: “Master of Science in Engineering, Civil Engineering” at The Faculty of Engineering at Lund University (LTH). The work was carried out in a collaboration between MAXLAB, Div. of Engineering Geology and Div. of Structural Mechanics.

I would like to thank my supervisor Nils Rydén for help with performing measurements and interpreting measurement data and especially for introducing me to the “world of measurements”. Thanks to Brian Norsk Jensen who has provided interesting and useful ideas and comments during the work. I would also like to thank Kent Persson for all help with the modelling and for always having the door open.

Special appreciation is directed towards Kjell Andersson for great help with the preparation of the measurements. Thanks also to the staff at the Div. of Structural Mechanics, e.g. Ola Flodén and Peter Persson for all support regarding Abaqus in the beginning of the work. And off course, thanks to all other, who in some way have been involved in the work!

I would also like to thank all friends and my family for all support during my entire education.

Finally I would like to thank Linda for all patience and encouragement.

Oskar Baggens
Summer 2012

Abstract

In the north-east part of Lund, Sweden, the MAX IV facility is (in the event of writing this thesis) under construction. MAX IV is a synchrotron radiation facility which has a high requirement regarding low vibrations.

Within this thesis a nearby road-bridge for the highway E22 was studied using experimental and numerical methods. The aim was to determine the magnitude of the road-bridge influence to the ground vibrations during passages of vehicles and thereby possibly explain the high levels of vibrations which have been measured during occasional events.

A finite element model of the road-bridge and surrounding soil was created using the software Abaqus. Material and soil-layering properties were defined according to a database which have been created during previous geotechnical studies. Geometry of the road-bridge was defined according to construction drawings.

The model was studied in two types of analysis; a steady-state and a transient analysis. The transient analysis was based on a load-case which was created in CALFEM/MATLAB using a simple standard axle model which was connected to a continuous beam model. A comparison between measurement data and modelling result was made. The comparison showed that the measured and predicted displacements of the road-bridge during a passage of a vehicle were approximately in the same magnitude.

Calculation of 1 s RMS levels of the vibration for the transient load-case at a specific point in the ground, identical to a stationary seismometer location, was done. The 1 s RMS value were below 20 nm in all three directions. It was therefore concluded that the suggested transient load-case not could explain the high levels of vibrations(>200 nm 1s RMS > 5 Hz) which had been measured previously.

Although the transient load-case approximated the passage of a vehicle fairly well it was concluded that a more refined load-case and model were needed in order to continue the investigation.

Sammanfattning

I nordöstra delen av Lund, Sverige, pågår (vid skrivande av det här arbetet) byggandet av MAX-IV. MAX-IV är en synkrotronljusanläggning med högt ställda krav vad gäller vibrationer.

Inom ramen för det här arbetet har en närbeliggande vägbro för motorvägen E22 studerats. Syftet var att undersöka vägbronns påverkan på markvibrationerna vid fordonspassager och om möjligt förklara de höga vibrationsnivåerna som stundtals uppmätts.

En finita element modell av vägbron och omgivande mark skapades i programmet Abaqus. Egenskaper för material och lagerföljder definierades enligt en databas som upprättats under tidigare studier. Vägbronns geometri definierades i enlighet med konstruktionsritningar.

Modellen studerades i två typer av analyser; en steady-state och en transient analys. Den transienta analysen baserades på ett lastfall som skapades i CALFEM/MATLAB med hjälp av en enkel modell av en standardaxel som var kopplad till en kontinuerlig balkmodell. En jämförelse mellan mätdata och beräknat resultat gjordes. Jämförelsen visade att uppmätta och beräknade förskjutningar av vägbron vid en fordonspassage var av ungefär samma storleksordning.

Beräkning av 1 s RMS värden gjordes för vibrationerna under det transienta lastfallet i en specifik punkt, identisk med placeringen av en stationär seismometer. 1 s RMS värdena var lägre än 20 nm i alla tre riktningar. Därmed ansågs inte det föreslagna transienta lastfallet kunna förklara de höga vibrationsnivåerna (>200 nm 1 s RMS > 5 Hz) som tidigare uppmätts.

Även då det transienta lastfallet approximerade passagen av ett fordon någorlunda väl var slutsatsen att lastfallet och modellen skulle behövas förfinas för att kunna fortsätta studien.

Contents

| | | |
|----------|---|-----------|
| 1 | Introduction | 1 |
| 1.1 | Background | 1 |
| 1.2 | Objective | 1 |
| 1.3 | Limitations | 1 |
| 1.4 | Outline | 2 |
| 2 | Description of the site | 3 |
| 2.1 | Road-bridge | 3 |
| 2.2 | Soil layer sequence and material properties | 5 |
| 2.3 | Material | 5 |
| 3 | Measurements | 7 |
| 3.1 | Measurement equipment | 7 |
| 3.2 | Measurement results | 10 |
| 3.2.1 | Frequency content | 10 |
| 3.2.2 | Displacement of measurement points | 17 |
| 4 | Theory | 23 |
| 4.1 | The Finite element method | 23 |
| 4.1.1 | Introduction | 23 |
| 4.1.2 | Equations of motion | 23 |
| 4.1.3 | FE-formulation | 24 |
| 4.2 | Structural dynamics | 27 |
| 4.2.1 | Equations of motion and finite element method for dynamic systems | 27 |
| 4.2.2 | Damping | 27 |
| 4.2.3 | Steady state response | 28 |
| 4.2.4 | Time integration | 28 |
| 4.3 | Finite element software implementations | 29 |
| 4.3.1 | Abaqus | 29 |
| 4.3.2 | CALFEM | 29 |
| 5 | Modelling | 31 |
| 5.1 | Geometry | 31 |
| 5.2 | Material and damping modelling | 35 |
| 5.3 | Element mesh and boundary conditions | 36 |
| 5.4 | Steady state analysis | 38 |
| 5.5 | Transient analysis | 39 |

| | | |
|----------|---|-----------|
| 5.5.1 | Axle model in CALFEM | 40 |
| 5.5.2 | Beam model in CALFEM | 41 |
| 5.5.3 | Connection of axle model and beam model | 44 |
| 5.5.4 | Defining transient load case in Abaqus | 48 |
| 6 | Modelling results | 51 |
| 6.1 | Definition of result points | 51 |
| 6.2 | Steady state analysis | 53 |
| 6.3 | Transient analysis | 55 |
| 6.3.1 | Response of road-bridge | 55 |
| 6.3.2 | Response of soil | 58 |
| 7 | Comparison of experimental and numerical results | 61 |
| 7.1 | Steady state analysis | 61 |
| 7.2 | Transient analysis | 65 |
| 8 | Conclusions and suggestions for further work | 73 |
| | Bibliography | 75 |

Chapter 1

Introduction

1.1 Background

MAX-lab is a Swedish laboratory in the field of Synchrotron Radiation Research, Nuclear Physics and Accelerator Physics. At the time of this study, the new generation of MAX-lab is under construction. The laboratory is planned to be operating by 2016. To ensure that MAX-lab will work properly high demands are stated regarding vibrational levels at the facility. Vibration sources may be installations in the facility and the people which are using it, but one possible major contributor is considered as the traffic nearby. Especially the influence from the highway E22 is a concern. Measurements are being made and have been made to study the levels of vibration in the ground and at the facility. Data shows that most of the times the vibration levels at MAX-lab is below the requirements stated. However, high vibrational levels are occasional observed. The origin of the high vibration levels have not yet been explained, although one suspicion is directed towards a road-bridge located at the highway E22.

1.2 Objective

This master thesis aims at analyse if the traffic load caused by moving vehicles passing the road-bridge may affect ground vibrations. If there is an influence, the objective is to determine the magnitude of the effect of the road-bridge on the ground vibrations.

1.3 Limitations

In the study the following assumptions and limitations were made:

- Selection of material parameters and soil-layering are chosen from a database which has been created during previous measurements.
- Measurements were performed at the road-bridge using four accelerometers at two measurement points.
- The model geometry of the road-bridge was defined according to construction drawings provided by the Swedish transport administration.

- The model was studied in a steady-state analysis and in a transient analysis.

1.4 Outline

The thesis is divided into the Chapters 2-8:

- In Chapter 2 the site and the road-bridge is presented.
- Measurements were taken at the road-bridge. The result from the measurements is presented in Chapter 3
- Chapter 4 gives theoretical background of the methods used in the study.
- In Chapter 5 the modelling procedure is presented.
- The result from the modelling is presented in Chapter 6.
- A comparison between measurement data and modelling result is presented in Chapter 7.
- Proposed suggestions for further work are presented in Chapter 8

Chapter 2

Description of the site

In this chapter, an overview of the site where the MAX-IV building site, the E22 and the road-bridge is located, is presented.

2.1 Road-bridge

The main focus in this study is directed towards a road-bridge located near the MAX-lab site. The road-bridge also acts as tunnel for a smaller road which passes the highway E22. The location of the road-bridge is shown in Figure 2.1 which is a map over the north-east part of the city Lund in Sweden.

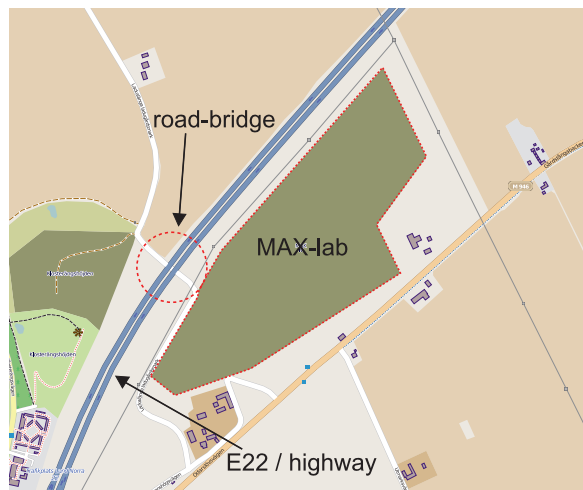


Figure 2.1: Location of the road-bridge

The Swedish transport administration provided the construction drawings of the road-bridge. The drawings provides information regarding the material and geometry of the road-bridge. The road-bridge is a casted concrete-frame and was built in the 1980s. The drawings revealed that an extension of the road-bridge was made in the 1990s, when the road was rebuilt and broaden. In

Figure 2.2, the studied road-bridge is shown in a photo taken in the winter of 2012.



Figure 2.2: Road-bridge in the winter of 2012

The cross-section of the road-bridge is shown in Figure 2.3. To be exact, it should be mentioned that in reality a small incline of the upper part of the roof of the road-bridge is present. The purpose of this incline is probably to prevent water from being trapped at the top. The incline is not present in the simplified section as shown in Figure 2.3. The length of the road-bridge perpendicular to the cross-section is 31 m.

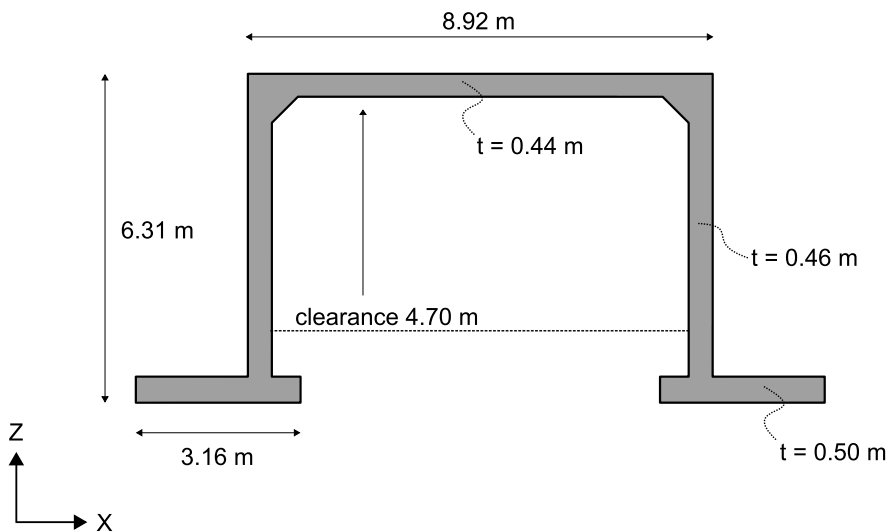


Figure 2.3: Cross-section of the road-bridge

2.2 Soil layer sequence and material properties

Knowledge about the soil layer sequence is very important in order to develop realistic simulation models. Field measurements have been made to determine the layer sequence and soil characteristics at the site around MAX-lab and the road-bridge. At the site of the road-bridge a relatively homogeneous clay layer has been found resulting in a simple approximation of the soil profile. The soil profile approximation is basically characterised by an 18 meter deep layer layer of clay situated the bedrock. An illustration of the layer sequence is shown in Figure 2.4.



Figure 2.4: Layer sequence

2.3 Material

The dynamic material properties for the road-bridge as well as for the surrounding ground are important information for the study of the road-bridge. Parameters regarding the soil characteristics are taken from the database that was created during previous studies which were aimed of ensuring acceptable vibration levels at the MAX-lab facility. By choosing the parameters according to that database it was easier to compare the results with investigations made previously. The database containing material data for the MAX-lab studies also contains information about suitable parameters for concrete and other materials such as asphalt.

In Table 2.1 the material parameters which are used in the modelling are shown. The quantities displayed in Table 2.1 are the materials density ρ [kg/m³], Young's modulus E [MPa], Poisson's ratio ν [-], Rayleigh damping parameter α [-], Rayleigh damping parameter β [-], damping ratio ζ [-].

| Material | ρ [kg/m ³] | E [MPa] | ν [-] | α [-] | β [-] | ζ [-] |
|----------|-----------------------------|-----------|-----------|--------------|-------------|-------------|
| Asphalt | 2600 | 5000 | 0.25 | 3.05 | 0.000589 | 0.05 |
| Concrete | 2400 | 40000 | 0.20 | 1.22 | 0.000235 | 0.02 |
| Clay | 2125 | 476 | 0.48 | 3.66 | 0.000707 | 0.07 |
| Bedrock | 2600 | 8809 | 0.40 | 1.22 | 0.000235 | 0.02 |

Table 2.1: Material data

Chapter 3

Measurements

Measurements of the vibration levels in the soil around MAX-lab have been performed and are continuously being performed with stationary seismometers. These seismometers record and transmits data continuously. Although the data from the seismometers contains a lot of information, a more specific measurement study was needed to investigate the behaviour of the road-bridge. Such new measurements at the road-bridge were made within the scope of this thesis. This chapter describes the procedure of a measurement that was made at the road-bridge.

3.1 Measurement equipment

The road-bridge response in terms of acceleration was registered during passages of vehicles on the highway. The measurements were done by using a data acquisition computer which gathered data from the accelerometers of the brand Wilcoxon model 731A. The Wilcoxon model 731A is an Ultra-quiet, ultra low frequency, seismic accelerometer which is a suitable measurement device for small accelerations at low frequencies. A picture of the accelerometer and corresponding amplifier system is shown in Figure 3.1. Four accelerometers were used simultaneously and positioned at two different measurement positions; one on the wall and one on the roof.



Figure 3.1: Wilcoxon model 731A

The positions of the accelerometers and the coordinate system orientation are shown in Figure 3.2. The two different positions are labelled *wall* and *roof*. The coordinate directions are labelled *1* and *3* which are the horizontal and vertical directions, respectively. The choice of coordinate system for the measurements was based on the horizontal plane being the XY-plane. This convention was also used for the modelling domain. At both positions, measurements were taken in the vertical (*3*) and the horizontal (*1*) direction parallel with the driving direction of the highway.

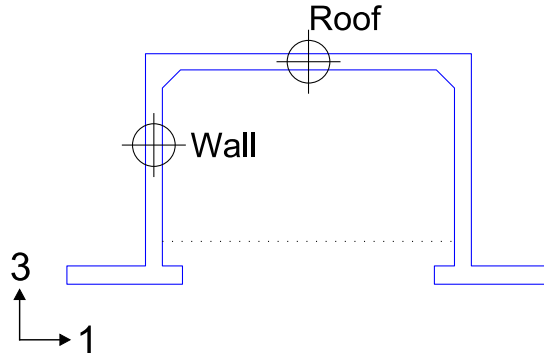


Figure 3.2: Measurement points

The accelerometers were mounted to quadratic metal tubes which in turn were attached to the road-bridge using glue and screws. A photo of the attachments of the accelerometers at the roof position and the wall position are shown in Figure 3.3 and Figure 3.4, respectively. In Figure 3.5 an overview of the two measurement points at the road-bridge is shown. In some photographs it is possible to identify stickers on the accelerometers displaying a number. This number should not be interpreted as a coordinate notation since it is an identity label of the accelerometer.



Figure 3.3: Attachment of accelerometers at the roof position



Figure 3.4: Attachment of accelerometers at the wall position



Figure 3.5: Overview of the measurement positions

It can also be noted that the accelerometers were mounted at the west side of the road bridge and that the wall position was located on the wall which the vehicles (on the western driving lanes) passes first. Measurements were recorded during 2 minute sessions and during this time the traffic on the road-bridge was captured with a simple handheld video recorder.

3.2 Measurement results

A total of 26 minutes of data were recorded. It is impossible to present all data in this thesis, therefore the following presentation will focus on the general observations that can be made from the data. Data collection from the accelerometers was performed during eight 2 minutes sessions and one 10 minute session. An example plots of the raw signals from the roof measurement point and the wall measurement point from one 2 minute measurement session are shown in Figure 3.6 and Figure 3.7, respectively. The variable $a7$ is a label for the current measurement session displayed.

During the measurements, vehicles were passing from both direction of the highway. One initial observation was that the southbound vehicles, i.e. the vehicles most closely to the measurement points, generated the highest response in terms of acceleration. From the raw signal it is also possible to conclude that the system is a highly damped system; the response during the passages of vehicles attenuates quickly.

3.2.1 Frequency content

The frequency content of a signal reveal a lot of the properties of the system which is studied. An effective way of displaying the frequency content of the signal is to produce spectrograms of the measured signals. The Figures 3.8-3.11 show spectrograms of the signals shown in Figure 3.6 and Figure 3.7. The window length of the spectrograms is one second.

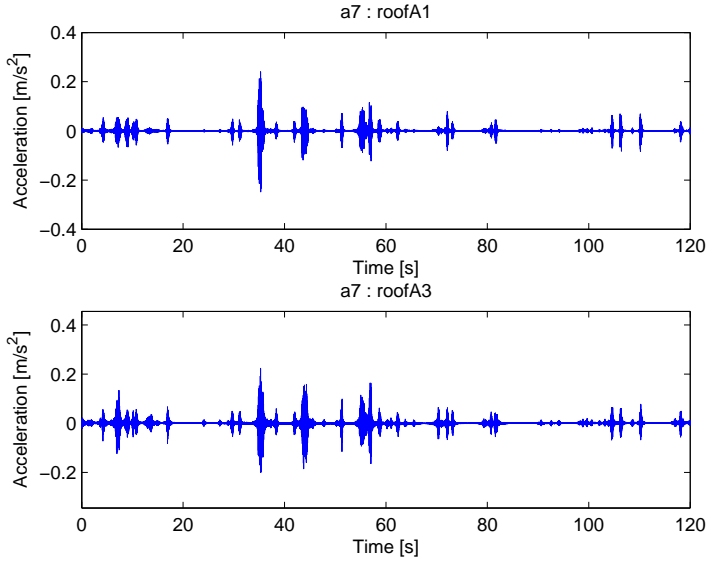


Figure 3.6: Raw signal from the roof measurement point

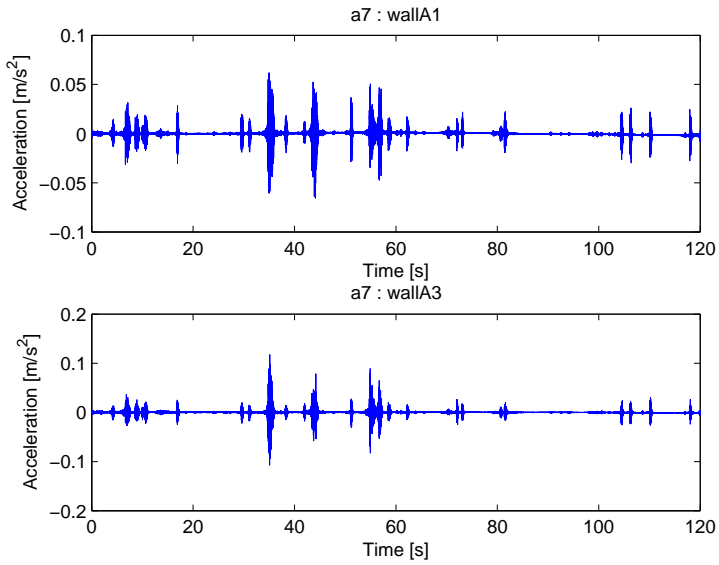


Figure 3.7: Raw signal from the wall measurement point

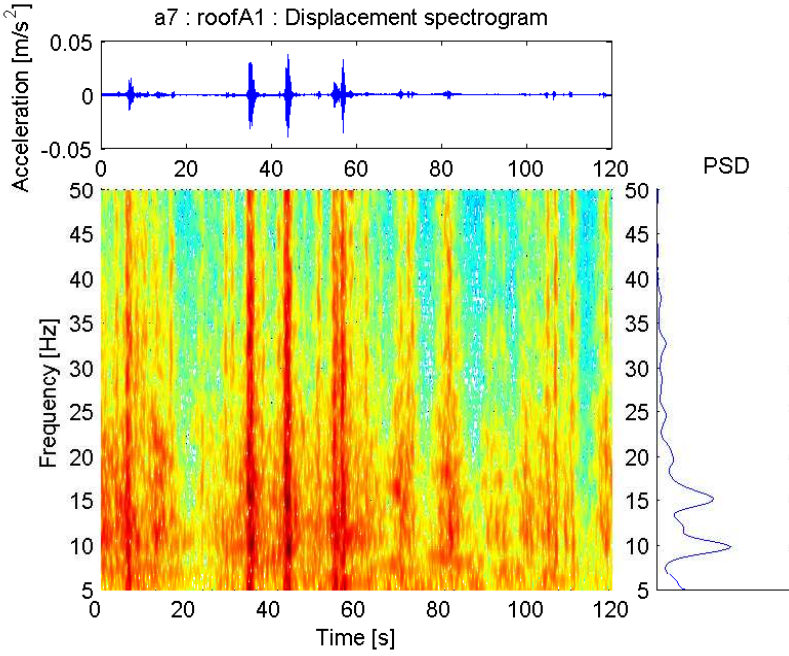


Figure 3.8: Displacement spectrogram of roof U1

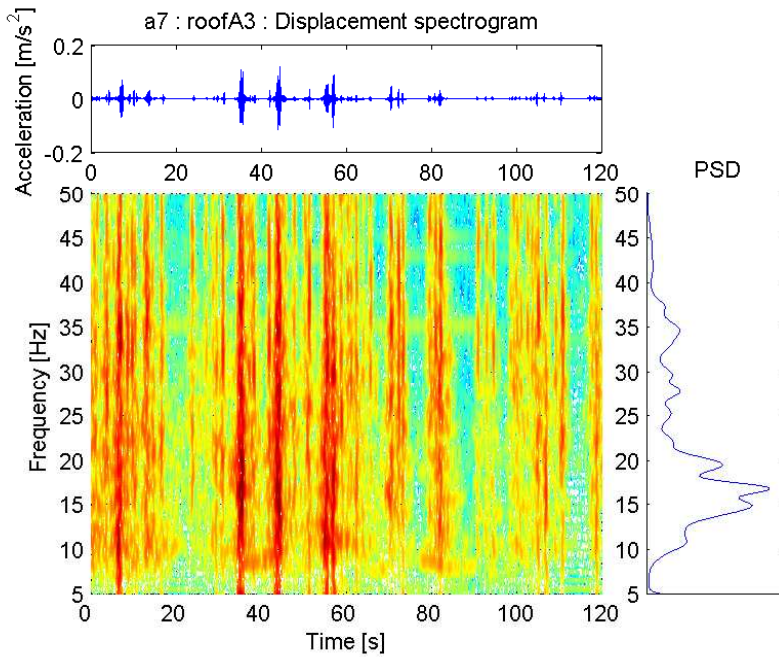


Figure 3.9: Displacement spectrogram of roof U3

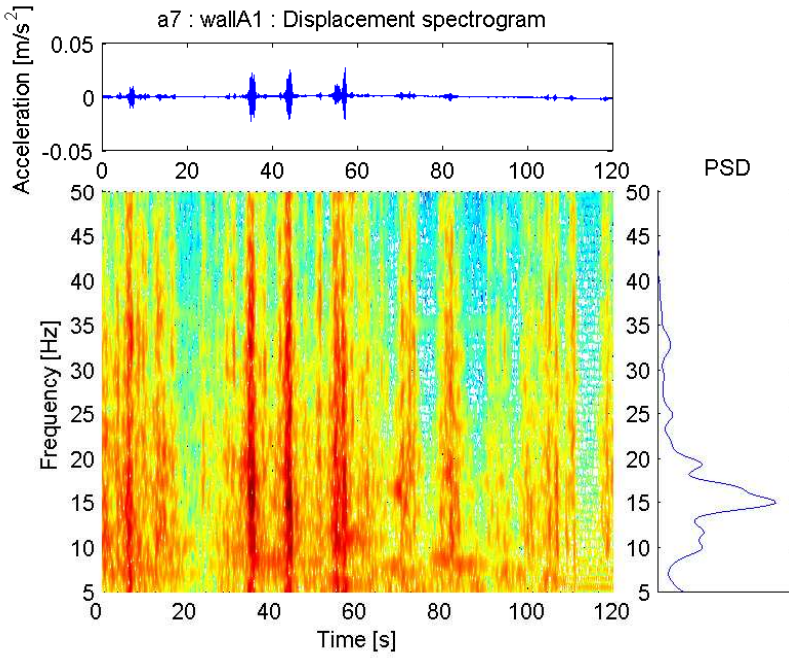


Figure 3.10: Displacement spectrogram of wall U1

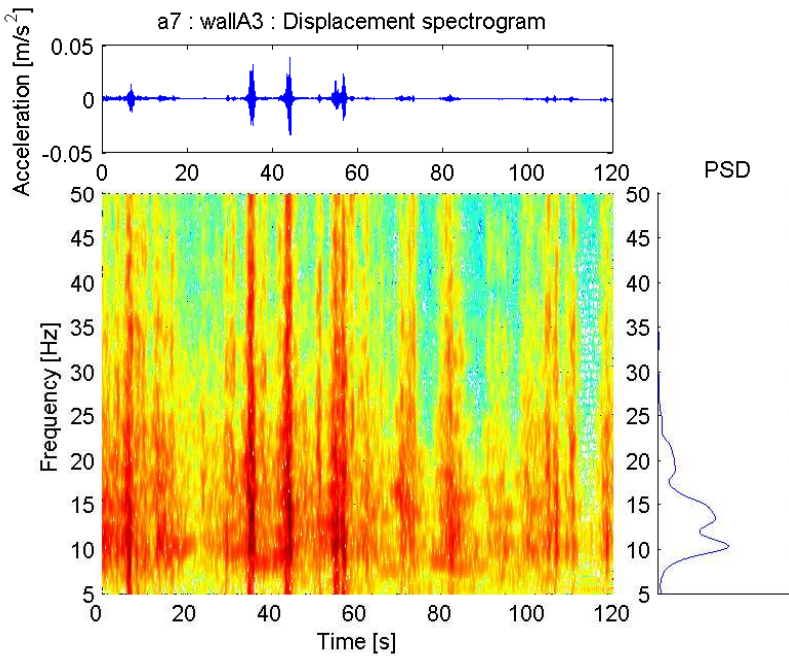


Figure 3.11: Displacement spectrogram of wall U3

The Figures 3.8-3.11 each contains three subfigures. The subfigure at the top shows the signal in time domain. The amplitude of the acceleration has decreased compared to the previous figure since the signal was lowpass filtered at 100 Hz with the aim of reducing high frequency content. The main subfigure contains the spectrogram of the signal. It is important to notice that the spectrogram is showing displacement amplitude instead of acceleration amplitude. The displacement amplitude $u_0(t, \omega)$ in the spectrogram is given by the relationship:

$$u_0(t, \omega) = \frac{a_0(t, \omega)}{\omega^2}$$

where $a_0(t, \omega)$ is the (measured) acceleration amplitude and ω is the corresponding angular frequency. The subfigure to the right of the main figure shows the power spectral density of the spectrogram. It should be mentioned that the frequencies below 5 Hz are not shown in the spectrogram since they tend to distort the scaling of the displacement amplitude due to their high magnitude.

It is clear from the spectrograms that higher magnitudes are reached during the passages of heavy vehicles. It is also evident that the frequency content during the passages is quite broadband and contains high amplitudes at a lot of frequencies. In general it is hard to determine some *unique* resonance frequencies which always are present during the passages. However, it is possible to identify a frequency response which is *more likely* to be present during the passages. The PSD plots can be used to evaluate which frequencies that in general have a higher response. All PSD-plots are normalized to have a maximum unit magnitude. The reason for using normalized PSD with unit magnitude instead of the original magnitude is to reduce the impact of single occasional events with extremely high amplitudes. The normalized PSD plots are shown in the following Figures 3.12-3.15. The average values of the PSD-plots are shown as a thicker line in the figures.

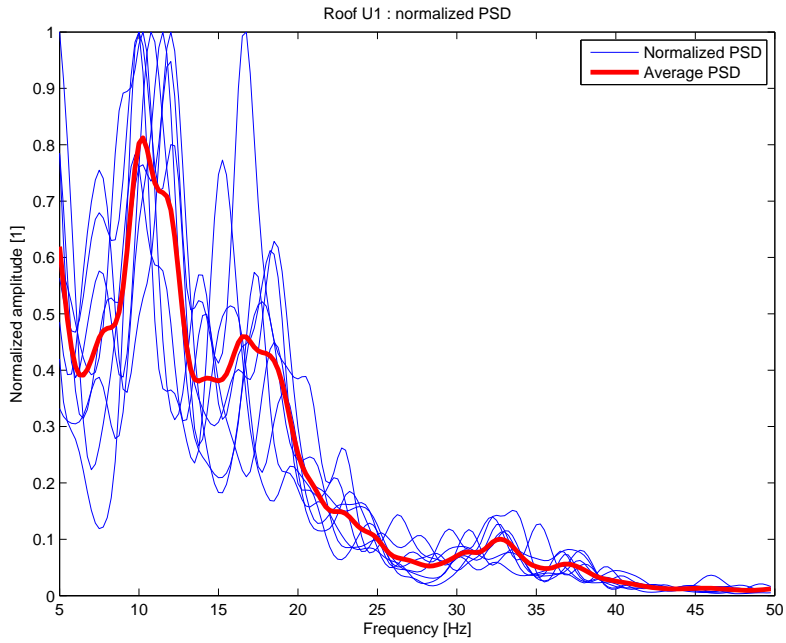


Figure 3.12: Normalized PSD of Roof U1

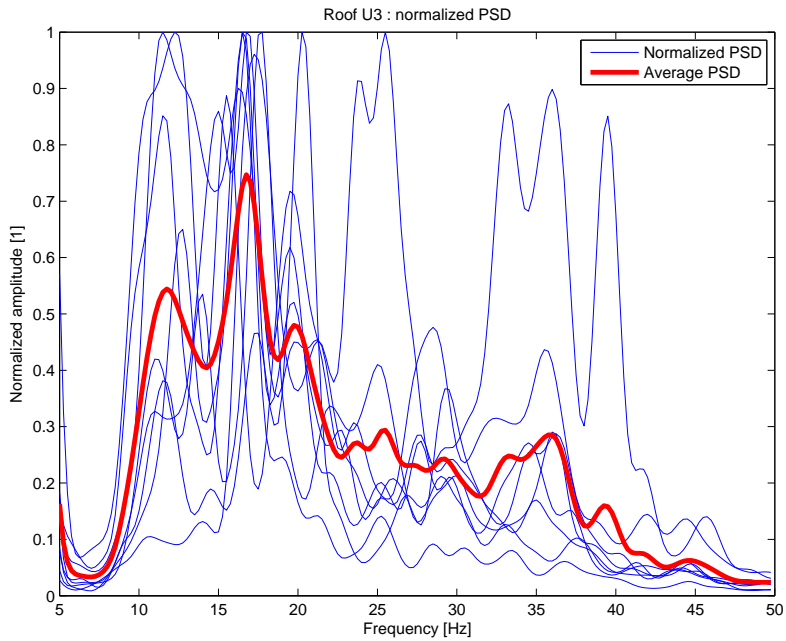


Figure 3.13: Normalized PSD of Roof U3

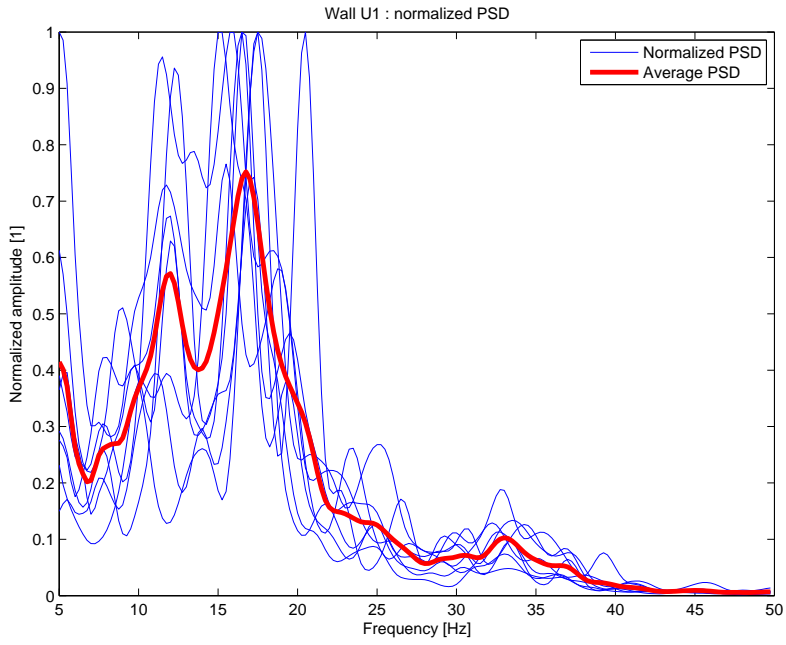


Figure 3.14: Normalized PSD of Wall U1

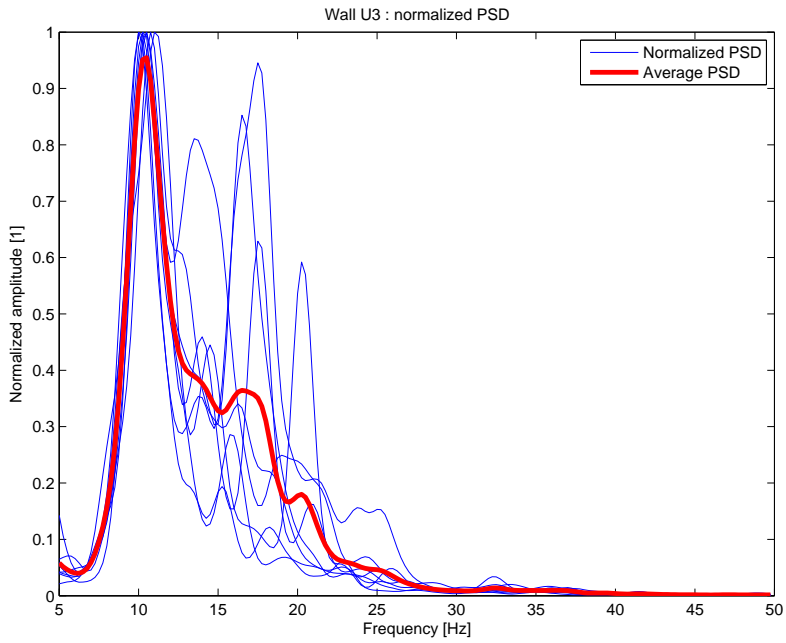


Figure 3.15: Normalized PSD of Wall U3

Although the response of the single PSD plots in Figure 3.12-3.15 varies it is still possible to identify frequency intervals which in general have higher amplitudes. An example of such an interval is shown in Figure 3.15 where an emphasized response is present around 11 Hz. A similar distinct response is more hard to identify in for example Figure 3.13. A possible explanation to why Figure 3.13 seem very randomized compared to Figure 3.15 may come from the nature of the load generated by a vehicle. The spectrogram indicates that the load is a complex combination of many frequencies. It is also reasonable to expect that the measurement point at the roof and especially the vertical direction is highly affected by this complex load. The complexity of the load comes probably from the fact that the vehicles are defined by different parameters such as the distance of the axles, the number of axles and the load on each axle which in general probably is not equal for all vehicles. The variation of these parameters may have important influence on the response of the road-bridge. Finally one may conclude that the road-bridge is mostly affected by frequencies lower than 40 Hz.

3.2.2 Displacement of measurement points

The displacement during a passage of a vehicle was determined from the recorded data by integration. Thereby the motion and location of the measurement positions as a function of time were established. Due to measurement noise, drift and rounding errors while performing numerical integration, the *whole continuous* displacement history during the *total* time history can not be shown. Focus is therefore directed to selected shorter time periods, i.e. the events of passing vehicles. During such shorter time periods the errors will be smaller thus making it possible to evaluate the motion of the measurement points. Two types of passages were studied; one passage of a southbound vehicle and one passage of a northbound vehicle.

Southbound vehicle

The passage of the southbound vehicle is labelled as *p18*, where *p* denotes *passage* and *18* is the number of the passage. The vehicle in the passage is a short truck with a fairly short axle spacing. A snapshot from the video recording showing the truck is shown in Figure 3.16.



Figure 3.16: Truck in southbound passage p18

The acceleration history of the passage is integrated and the displacement history for the local time interval of the passage is derived. It should be noted that a change of axis have been made in the following plots which contains the horizontal time history of displacement. The x- and y-axis are switched in order to make the direction of the displacement more intuitive. The displacement histories of the measurement point at the roof and at the wall is shown in Figure 3.17 and Figure 3.18, respectively.

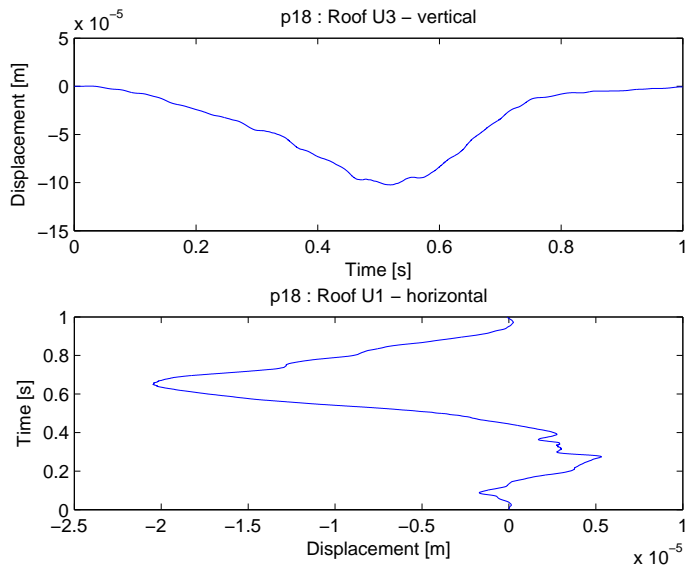


Figure 3.17: Time histories of the displacements at the roof measurement point

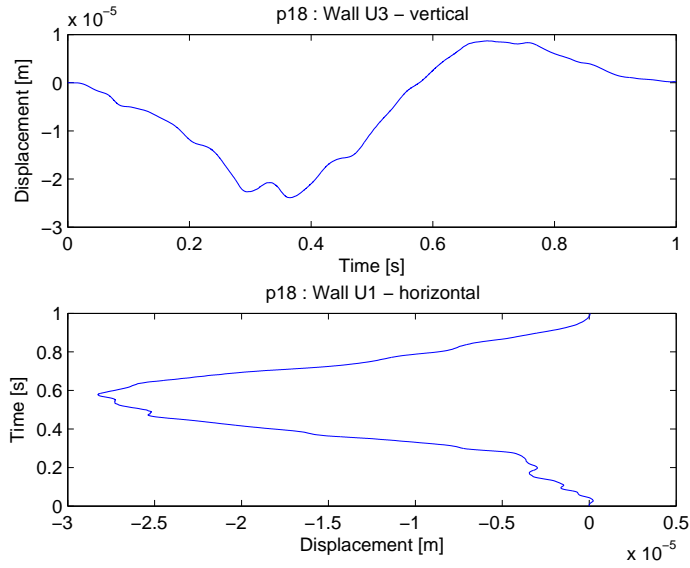


Figure 3.18: Time histories of the displacements at the wall measurement point

An appealing way of presenting the displacements shown in Figures 3.17-3.18 are to display them in a plot with the road-bridge included. Such a plot is shown in Figure 3.19.

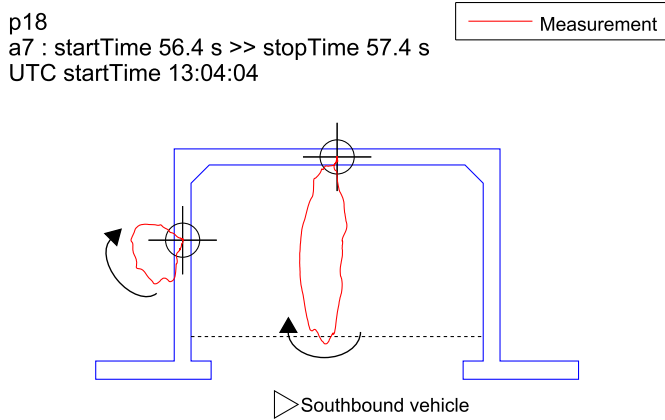


Figure 3.19: Illustration of movement of the measurement points

Northbound vehicle

An illustration was also made for the northbound vehicle as shown in Figure 3.20. The truck for the passage p32 has, as the truck for p18, a relative short axle spacing.



Figure 3.20: Truck in northbound passage p32

The displacement time history is shown in Figures 3.21-3.22. A change of axis for the horizontal displacement time history was made as for the previous plot.

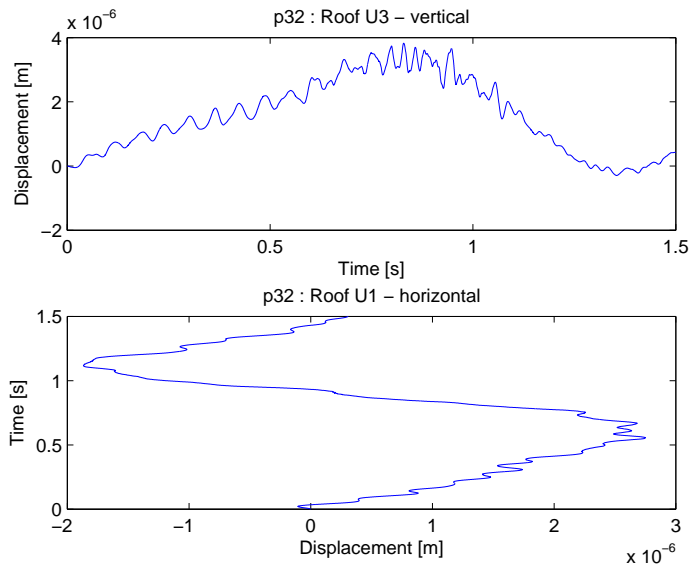


Figure 3.21: Time histories of the displacements at the roof measurement point

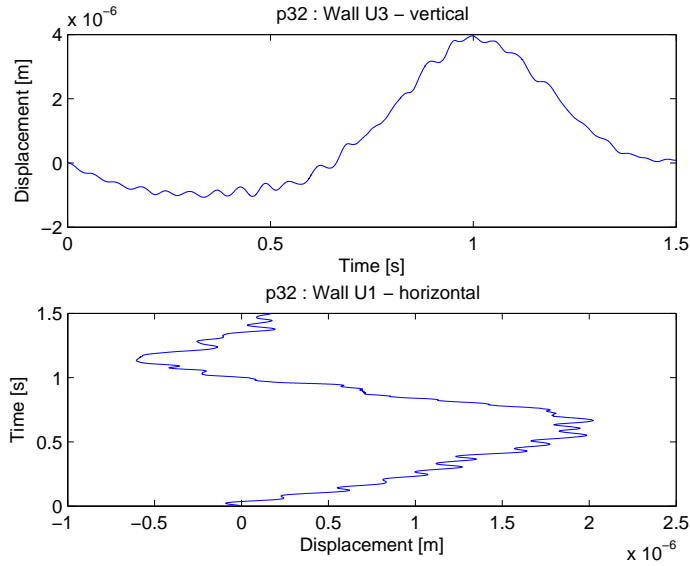


Figure 3.22: Time histories of the displacements at the wall measurement point

One important observation that can be made from the Figures 3.21-3.22 is that the displacement may be divided into a quasi-static displacement and a dynamic displacement. The quasi-static displacement constitutes the main part of the total displacement whereas the dynamic displacement generates small oscillations around the current position. The reason why it is easier to identify the two components of the displacement for the passage p32 of the northbound vehicle compared to the southbound passage p18 is because the quasi-static amplitude is smaller and thereby not hiding the dynamic displacement. An explanation to why the quasi-static displacement is smaller originates from the fact that the vehicle was moving on the driving lane located farthest from the measurement points. It is therefore reasonable to expect a response with smaller amplitudes. A combination of the previous plots is shown in Figure 3.23 where it should be noted that a different scale factor was used as in Figure 3.19.

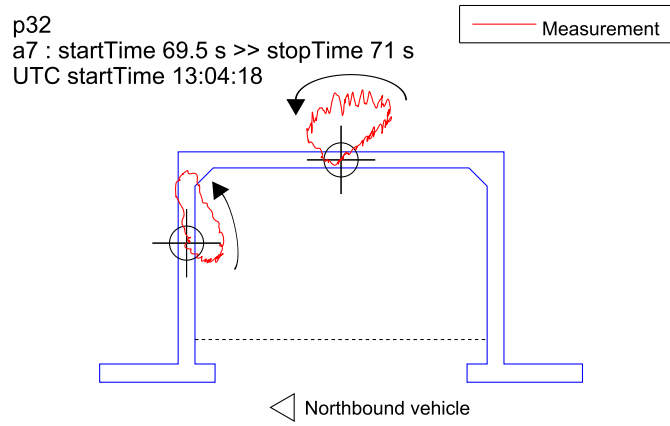


Figure 3.23: Illustration of movement of the measurement points

Chapter 4

Theory

This chapter gives a general overview of the theory and methods used in the study. The chapter consist mainly of three sections where the first section describes the basis of the Finite element method. The second second discuss some of the topics of structural dynamics and how the Finite element method can be used for dynamic problems. The third and last section gives a brief overview of the Finite element software implementations which are adopted in the study.

4.1 The Finite element method

4.1.1 Introduction

The main numerical tool used in this master thesis is the Finite element method, often abbreviated as FEM. In some sense using FEM can be seen as describing (i.e. to build) an object by connecting small pieces together (finite elements), which in unity, make a fair approximation of the total object. By using sufficiently small elements it is possible to capture the real behaviour of the main object with small errors. One of the most significant advantages of FEM is the ability to describe arbitrary objects with high precision. It can be shown that with increasing number of elements i.e. a finer element mesh, the solution converges towards the *exact* analytical solution of the problem. However, finite element model with many elements will have a high computational cost. Consequently FEM gives the possibility of studying objects for which there may not exist an analytical solution. Nowadays FEM is one of the most used engineering tools world-wide.

This chapter gives a brief overview of the derivation of a FEM-formulation. For a more detailed description see standard textbooks on the subject such as (Zienkiewicz and Taylor, 2000).

4.1.2 Equations of motion

To establish a FEM-formulation one needs to initially consider an arbitrary body subjected to a body force b_i (unit N/m^3) and a traction vector t_i (unit N/m^3) (Ottosen and Ristinmaa, 2005), see Figure 4.1. The subscript i represents an index, $i = 1, 2, 3$ each denoting one coordinate axis, i.e. b_i and t_i are

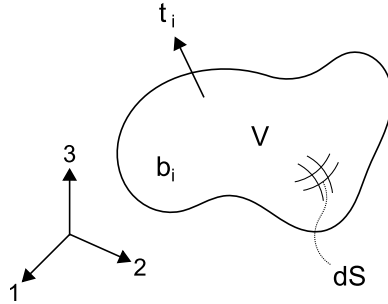


Figure 4.1: Newton's second law for an arbitrary body

quantities which both consists of three parts, where each component represents the magnitude of the quantity in respective direction. To fulfill Newton's second law, the following equation must be satisfied:

$$\int_S t_i dS + \int_V b_i dV = \int_V \rho \ddot{u}_i dV \quad (4.1)$$

where u_i is the displacement and ρ is the density. In eq. 4.1 the dot (\dot{u}_i) sign above u_i specifies a differentiation with respect to time, i.e. \ddot{u}_i represents acceleration. The traction vector t_i is given by following expression:

$$t_i = \sigma_{ij} n_j \quad (4.2)$$

where σ_{ij} is a stress tensor. Insertion of eq. 4.2 into eq. 4.1 gives:

$$\int_S \sigma_{ij} n_j dS + \int_V b_i dV = \int_V \rho \ddot{u}_i dV$$

By use of Gauss divergence theorem, the surface integral can be transformed to a volume integral and the following relation is obtained:

$$\int_V (\sigma_{ij,j} + b_i - \rho \ddot{u}_i) dV = 0$$

Since the relation should hold for arbitrary volumes it can be concluded that the following equations, i.e. the equations of motion, always must be satisfied:

$$\sigma_{ij,j} + b_i = \rho \ddot{u}_i \quad (4.3)$$

4.1.3 FE-formulation

The equations of motion in eq. 4.3 describes an equilibrium relation at an infinitesimal point. This relation can be transformed into a so called weak formulation. It is done by multiplying eq. 4.3 with an arbitrary *virtual* displacement field v_i and integrating over the volume, i.e. we get:

$$\int_V v_i (\sigma_{ij,j} + b_i - \rho \ddot{u}_i) dV = 0$$

The word *virtual* is used to emphasize that the displacement field is a fictitious quantity, which is not the same as the *real* displacement field. By use of the chain rule the expression can be rewritten into:

$$\int_V [(\sigma_{ij}v_i)_{,j} - \sigma_{ij}v_{i,j}]dV + \int_V (v_i b_i - \rho v_i \ddot{u}_i)dV = 0 \quad (4.4)$$

With the Gauss theorem and eq. 4.2, the following identity can be established:

$$\int_V (\sigma_{ij}v_i)_{,j}dV = \int_S \sigma_{ij}v_i n_j dS = \int_S v_i t_i dS$$

which inserted into eq. 4.4 gives:

$$\int_V \rho v_i \ddot{u}_i dV + \int_V v_{i,j} \sigma_{ij} dV = \int_V v_i t_i dS + \int_V v_i b_i dV \quad (4.5)$$

In mechanics the small strain tensor ϵ_{ij} is given by the expression:

$$\epsilon_{ij} = \frac{1}{2}(u_{i,j} + u_{j,i}) \quad (4.6)$$

where u_i is the displacement field of the body. By switching indices, it is evident that the small strain tensor is symmetric, i.e. $\epsilon_{ij} = \epsilon_{ji}$. It can also be shown that an analogous symmetry exist for the stress tensor as well, i.e. $\sigma_{ij} = \sigma_{ji}$. In eq. 4.4 an arbitrary *virtual* displacement field was introduced and in a similar manner there is no restriction to introduce a *virtual* strain related to the *virtual* displacement field:

$$\epsilon_{ij}^v = \frac{1}{2}(v_{i,j} + v_{j,i}) \quad (4.7)$$

With eq. 4.7, eq. 4.5 turns into:

$$\int_V \rho v_i \ddot{u}_i dV + \int_V \epsilon_{ij}^v \sigma_{ij} dV = \int_V v_i t_i dS + \int_V v_i b_i dV \quad (4.8)$$

which is the weak form of the equations of motion.

The finite element method is a numerical tool which is practically implemented in computer code. It is therefore suitable to define some matrices which makes it easy to implement FEM with standard matrix operations. The following matrices are defined:

$$\epsilon^v = \begin{bmatrix} \epsilon_{11}^v \\ \epsilon_{22}^v \\ \epsilon_{33}^v \\ 2\epsilon_{12}^v \\ 2\epsilon_{13}^v \\ 2\epsilon_{23}^v \end{bmatrix}; \quad \sigma = \begin{bmatrix} \sigma_{11} \\ \sigma_{22} \\ \sigma_{33} \\ \sigma_{12} \\ \sigma_{13} \\ \sigma_{23} \end{bmatrix}; \quad \ddot{\mathbf{u}} = \begin{bmatrix} \ddot{u}_1 \\ \ddot{u}_2 \\ \ddot{u}_3 \end{bmatrix}$$

$$\mathbf{v} = \begin{bmatrix} v_1 \\ v_2 \\ v_3 \end{bmatrix}; \quad \mathbf{t} = \begin{bmatrix} t_1 \\ t_2 \\ t_3 \end{bmatrix}; \quad \mathbf{b} = \begin{bmatrix} b_1 \\ b_2 \\ b_3 \end{bmatrix}$$

In FEM the objective is to make an approximation of the displacement by interpolating values at node points with weight function, i.e. so called shape functions. The displacements are approximated by the following expression:

$$\mathbf{u}(x_i, t) = \mathbf{N}(x_i) \mathbf{a}(t) \quad (4.9)$$

where \mathbf{N} are the shape functions which approximate the values \mathbf{a} at the nodal-points. The accelerations are approximated in a similar manner:

$$\ddot{\mathbf{u}}(x_i, t) = \mathbf{N}(x_i) \ddot{\mathbf{a}}(t) \quad (4.10)$$

A relationship between the displacements and the strain was given in eq. 4.6. If the displacements are known it is obviously possible to determine the corresponding state of strain. The calculation of the strain can therefore be approximated by the following expression:

$$\epsilon = \mathbf{B}(x_i) \mathbf{a}(t) \quad (4.11)$$

where \mathbf{B} are shape functions derived from differentiation of \mathbf{N} according to eq. 4.6.

In eq. 4.8 a virtual displacement field v_i was introduced. In FEM a particular choice of the approximation of the virtual displacements is done according to the Galerkin method:

$$\mathbf{v} = \mathbf{N} \mathbf{c} \quad (4.12)$$

where c is vector containing arbitrary displacement values, which may be interpreted as arbitrary constants. In conformity with eq. 4.11 the virtual strain is approximated by:

$$\epsilon^v = \mathbf{B} \mathbf{c}. \quad (4.13)$$

Going back to the virtual work expression in eq. 4.8 and introducing the matrix formulation we get the following expression:

$$\int_V \rho \mathbf{v}^T \ddot{\mathbf{u}} dV + \int_V \epsilon_v^T \sigma dV = \int_S \mathbf{v}^T \mathbf{t} dS + \int_V \mathbf{v}^T \mathbf{b} dV$$

By inserting eq. 4.10, 4.12-4.13 the expression turns into:

$$\mathbf{c}^T \left\{ \int_V \rho \mathbf{N}^T \mathbf{N} dV \ddot{\mathbf{a}} + \int_V \mathbf{B}^T \sigma dV - \int_S \mathbf{N}^T \mathbf{t} dS - \int_V \mathbf{N}^T \mathbf{b} dV \right\} = 0.$$

This expression should hold for any c , therefore the following equations always have to be fulfilled:

$$\int_V \rho \mathbf{N}^T \mathbf{N} dV \ddot{\mathbf{a}} + \int_V \mathbf{B}^T \sigma dV = \int_S \mathbf{N}^T \mathbf{t} dS + \int_V \mathbf{N}^T \mathbf{b} dV$$

Assuming that a constitutive relation exists which relates the stresses and the strains, such as Hooke's law in the case of linear elasticity, that can be written (by use of eq. 4.11) on the form of

$$\sigma = \mathbf{D} \epsilon = \mathbf{D} \mathbf{B} \mathbf{a}$$

it is possible to finally write the finite element formulation:

$$\mathbf{M} \ddot{\mathbf{a}} + \mathbf{K} \mathbf{a} = \mathbf{f} \quad (4.14)$$

where

$$\mathbf{M} = \int_V \rho \mathbf{N}^T \mathbf{N} dV; \quad \mathbf{K} = \int_V \mathbf{B}^T \mathbf{D} \mathbf{B} dV; \quad \mathbf{f} = \int_S \mathbf{N}^T \mathbf{t} dS + \int_V \mathbf{N}^T \mathbf{b} dV$$

4.2 Structural dynamics

4.2.1 Equations of motion and finite element method for dynamic systems

Initially we consider a single degree of freedom system, a so called SDOF-system. The SDOF-system is characterised by only having possibility to move in one *single* direction.

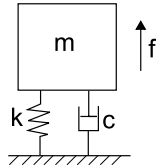


Figure 4.2: Single degree of freedom, SDOF-system

For a SDOF system as shown in Figure 4.2 the equation of motion, in its most simple form, is written as:

$$m\ddot{u} + c\dot{u} + ku = f$$

where m is the mass of the system, c is a viscous damping coefficient and k is the spring stiffness. It appears that the equation of motion for the SDOF-system is very similar to the finite element formulation given in 4.14, with the difference of the viscous damping term. However there is no restriction to add a damping term to the finite element formulation and write:

$$\mathbf{M}\ddot{\mathbf{a}} + \mathbf{C}\dot{\mathbf{a}} + \mathbf{K}\mathbf{a} = \mathbf{f} \quad (4.15)$$

which is the finite element formulation for a dynamic system with damping. How the damping matrix \mathbf{C} is established varies but one common method is assuming damping according the method given by Rayleigh, the so called Rayleigh damping, which is described in following section.

4.2.2 Damping

Damping is, in general, a quantity which is hard to describe in the same well-defined ways as mass or stiffness (Chopra, 1995). The reason why it is hard to model damping comes from the fact that the mechanics of damping, which results in the loss of energy, is extremely complicated and not always well defined. Since the damping property is desirable in the study of structural dynamics several alternative solutions have been developed to take into account structural damping. One of the most used methods for creating structural damping is the Rayleigh damping. The basis of Rayleigh damping is that structural damping can be seen as a combination of a mass proportional part and a stiffness proportional part. Neither of the assumptions, on its own, describes damping in an appealing way. Experience has fortunately shown that the assumptions, combined together, works well practically.

In a mathematical context the Rayleigh damping takes the following form:

$$\mathbf{C} = \alpha\mathbf{M} + \beta\mathbf{K} \quad (4.16)$$

where α and β are the mass proportional and stiffness proportional parameters, respectively. One can show that the damping ratio ζ , if Rayleigh damping is used, at the angular frequency ω can be calculated by:

$$\zeta = \frac{\alpha}{2} \frac{1}{\omega} + \frac{\beta}{2} \omega. \quad (4.17)$$

The problem of estimating damping is therefore reduced to the task of making appropriate choices of the parameters α and β . By field studies as well as experience the choices are made to give a desired damping ratio in a specific frequency interval.

4.2.3 Steady state response

A common problem statement in structural dynamics concerns the response to harmonic excitation. If the responses for harmonic excitation at different forcing frequencies are known it is possible to give an indication of the structural response at arbitrary forcing load cases. In general the amplitude and shape of the structural response varies with different forcing frequencies. Of special interest is knowledge about which frequencies where high magnitudes are received, i.e. to know which forcing frequencies that coincides with the structural resonance frequencies.

A dynamic system which is subjected to a harmonic force with the forcing frequency ω can in general be described by the following equations:

$$\mathbf{M}\ddot{\mathbf{u}} + \mathbf{C}\dot{\mathbf{u}} + \mathbf{K}\mathbf{u} = \mathbf{f}_0 e^{i\omega t} \quad (4.18)$$

It can be shown that the structural response will oscillate at the same frequency as the forcing frequency (with a phase lag if damping is present). The displacement may then be described by the following complex notation:

$$\mathbf{u} = \mathbf{u}_0 e^{i\omega t}$$

where \mathbf{u}_0 is the complex amplitude. By differentiation of \mathbf{u} we get:

$$\dot{\mathbf{u}} = i\omega \mathbf{u}_0 e^{i\omega t}; \quad \ddot{\mathbf{u}} = -\omega^2 \mathbf{u}_0 e^{i\omega t}$$

Insertion into eq. 4.18 yields:

$$(-\omega^2 \mathbf{M} + i\omega \mathbf{C} + \mathbf{K})\mathbf{u}_0 = \mathbf{f}_0 \quad (4.19)$$

which is an equation with no time dependency. By solving the system, the complex displacement amplitude \mathbf{u}_0 is determined. The complex displacement amplitude also provides information of how the phase of the structural displacements is related to the phase of the exciting force.

4.2.4 Time integration

The previous section dealt with the problem concerning structural response at harmonic loads. In reality the forcing load can take an arbitrary form. To study structural systems subjected to arbitrary time varying forces one has to

adopt other solution techniques. An often used numerical solution procedure for evaluating equations such as:

$$\mathbf{M}\ddot{\mathbf{u}} + \mathbf{C}\dot{\mathbf{u}} + \mathbf{K}\mathbf{u} = \mathbf{f}(t). \quad (4.20)$$

is the Newmark method (Krenk, 2009). There are many other algorithms which can handle time stepping, but basically the essence of those solution procedures are still based on, or are very close to, the Newmark method. Therefore one often talk about the “Newmark family” of methods. The main assumption in the Newmark method is that, given the present time t_n , it is possible to find the displacements and velocities at the next time step $t_{n+1} = t_n + h$, where h is the time step length. By using:

$$\dot{u}_{n+1} = \dot{u}_n + (1 - \gamma)h\ddot{u}_n + \gamma h\ddot{u}_{n+1} \quad (4.21)$$

$$u_{n+1} = u_n + h\dot{u}_n + \left(\frac{1}{2} - \beta\right)h^2\ddot{u}_n + \beta h^2\ddot{u}_{n+1} \quad (4.22)$$

where α and β are parameters that control how the solution are going to map towards the present state and the next step, the solution at the next time step may be found.

4.3 Finite element software implementations

A great number of softwares which in some way are based on the finite elements method exist. There are both general finite element software which treats a wide range of problems and software which is more directed towards specific problems. In this thesis two software implementations have been used; Abaqus and CALFEM.

4.3.1 Abaqus

Abaqus FEA (hereby after only Abaqus) is a commercial FEM-code software. Abaqus consists of four main parts: Abaqus/CAE, Abaqus/CFD, Abaqus/Standard and Abaqus/Explicit. The Abaqus/CAE-part (computer aided engineering) is used for pre-processing and post-processing i.e. to create an input file to one of the analyzers Abaqus/CFD, Abaqus/Standard or Abaqus/Explicit which perform the analysis, the result is finally viewed in Abaqus/CAE. In this report Abaqus/CAE and Abaqus/Standard are used. Abaqus/CFD is used for Computational Fluid Mechanics and Abaqus/Explicit is based on explicit time integration and is used for short time transient events analysis such as car-crash simulations). Abaqus is consequently a very general finite element software which makes it possible to use it to study a wide spectrum of engineering problems. This fact is probably one of the main reason why the software requires much practise before one can perform an analysis, especially if one wishes to carry out more complicated and customised analysis.

4.3.2 CALFEM

CALFEM is a finite element program which is implemented as a toolbox in MATLAB (there are some other language implementations, but the main usage

is with MATLAB) (Austrell et al., 2004). The toolbox contains a set of finite element analysis subroutines. There exist unlimited possibilities to customise the routines as well as writing own subroutines. However, these customising features comes to the price of that the size of the problems and the complexity of the geometry somehow must be at a reasonable level.

Chapter 5

Modelling

This chapter describes the modelling of the road-bridge which was analysed with finite element calculations. The commercial code Abaqus FEA as well as the educational MATLAB toolbox CALFEM were used for the analyses. Abaqus was used as the main computational tool for the finite element analysis while CALFEM was used to develop a load case for the transient analysis which was studied with use of Abaqus.

5.1 Geometry

The modelling domain was created as a block with the size of $230 \times 215 \times 100 \text{m}^3$. A causeway was created upon the surface of the block. At the centre of the causeway and the block, the road-bridge was created. An overview of the modelling domain is shown in Figure 5.1.

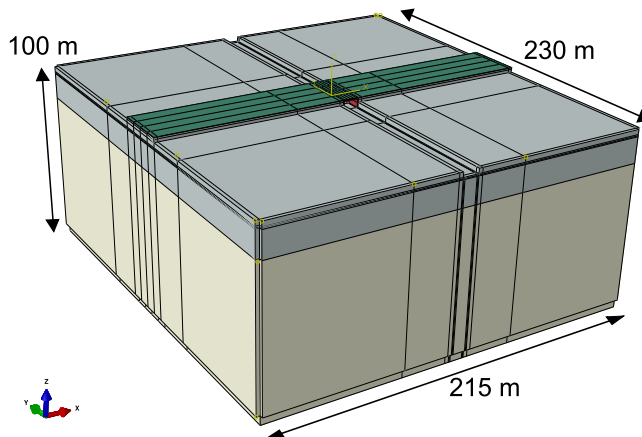


Figure 5.1: Modelling domain

In Figure 5.2 a view of the XY-plane is shown. The XY-plane is chosen as the ground surface. In Figure 5.3 a view of the XZ-plane is shown. The traffic direction of the causeway is parallel with the X-axis. At the bottom of the block the bedrock is located followed by a layer of clay (clay till). Upon the layer of clay the causeway was created, which was assumed to consist of clay as well. On top of the causeway a thin layer of asphalt was modelled. In Figure 5.4 a section of the block in the YZ-plane is shown. The YZ-plane represents the plane where the traffic direction of the causeway is perpendicular.

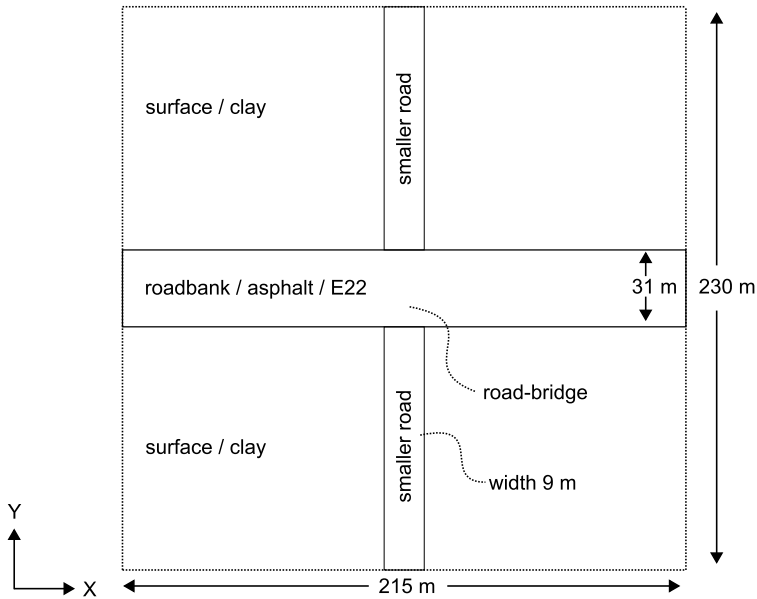


Figure 5.2: Modelling section XY-plane

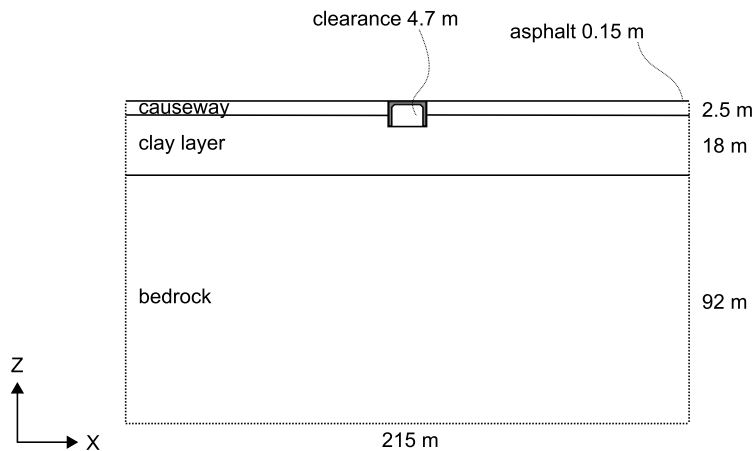


Figure 5.3: Modelling section XZ-plane

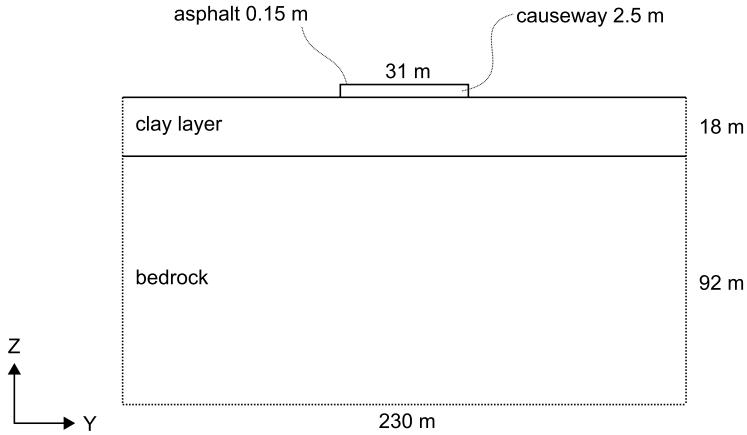


Figure 5.4: Modelling section YZ-plane

The Swedish transport administration provided construction drawings of the road-bridge. These construction drawings were the base for the modelling description of the road-bridge. The road-bridge was created in Abaqus as a homogeneous solid concrete part according to the section which is shown in Figure 5.5. The modelled section was almost the same as in the construction drawings. The difference was that the road-bridge in the construction drawings had a small incline at the top, probably in order to avoid that water got trapped on top of the construction. This feature was not modelled since the incline was assumed to have no effect on the frequencies utilised in this study.

In section 2.1 it was mentioned that an extension of the road-bridge was made at a later date. It would need detailed investigations to fully describe the connection between the old and the new part of the road-bridge. Therefore it was assumed that the two parts have a full interaction to each other. The road-bridge was also assumed to have a full interaction to the surrounding materials as well. In Abaqus modelling terms, one single part was created and thereafter partitioned into the different material and geometry definitions. The reinforcement steel was not taken into account when modelling the road-bridge, since small deformations were assumed. The partitioned geometry of the road-bridge is shown in Figure 5.6.

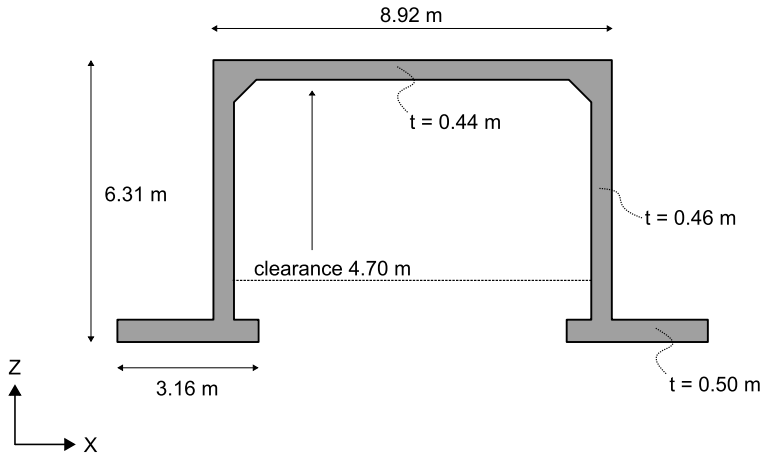


Figure 5.5: Section of road-bridge

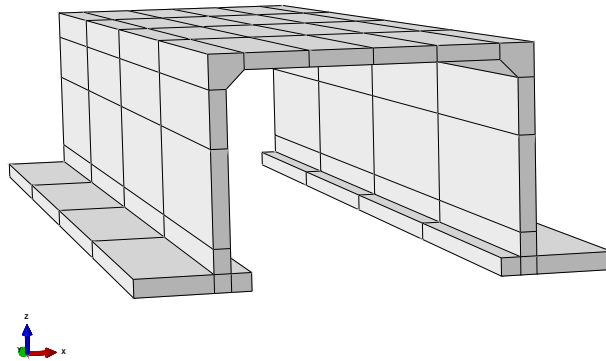


Figure 5.6: Geometry of the road-bridge

5.2 Material and damping modelling

In the model four different material definitions were applied: asphalt, concrete, clay and bedrock. The properties of the material is shown in Table 2.1. The damping is in the steady state analysis modelled with a stiffness proportional damping matrix using the loss factor η . The usage of this kind of damping leads to a slightly reformulation of the system that were solved, i.e. eq. 4.19 is written as:

$$(-\omega^2\mathbf{M} + \mathbf{K}^*)\mathbf{u}_0 = \mathbf{f}_0$$

where

$$\mathbf{K}^* = \mathbf{K}(\mathbf{I} + i\eta).$$

The loss factor η is calculated as:

$$\eta = 2\zeta$$

In the transient analysis the damping was modelled with Rayleigh damping. As mentioned in section 4.2.2 it is possible to evaluate eq. 4.16 to study the damping ratio as a function of the frequency. By using the Rayleigh damping parameters given in Table 2.1 one can create the diagram shown in Figure 5.7, which illustrates the damping as a function of frequency for respective material definition. From Figure 5.7 it is possible to observe that the clay material is modelled with strong damping properties.

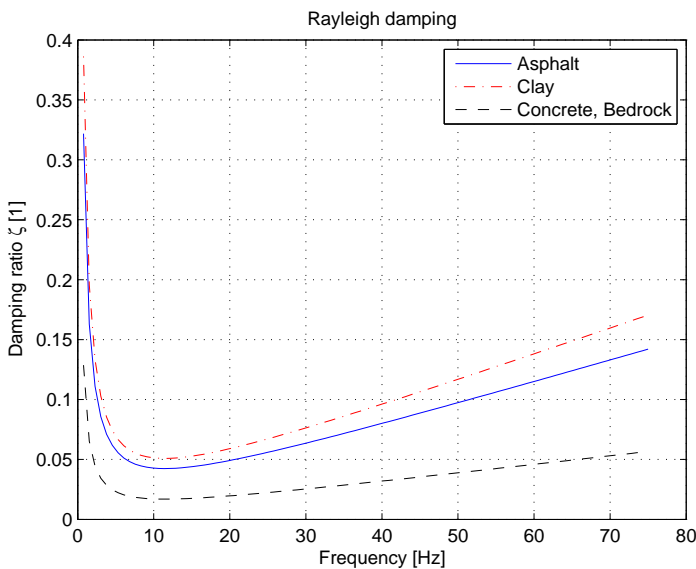
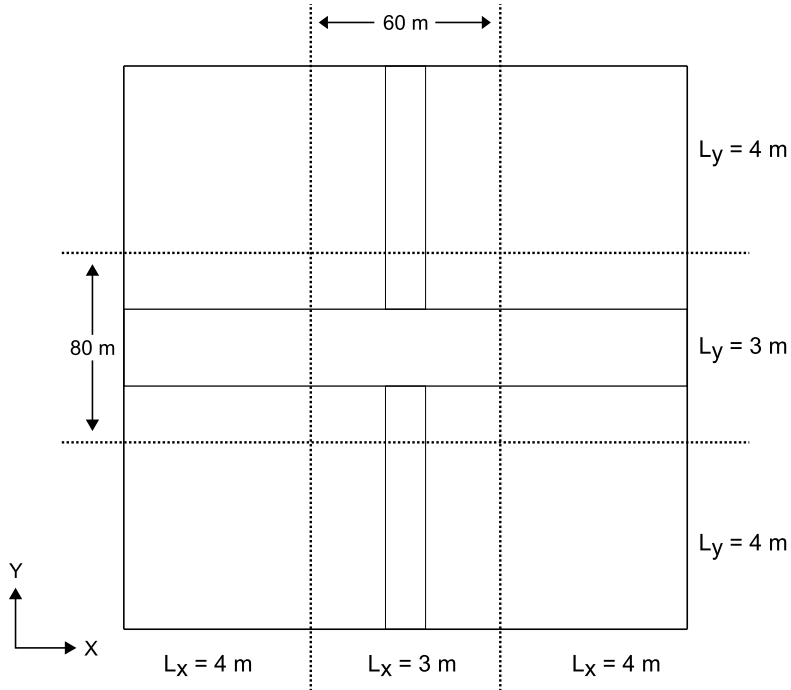
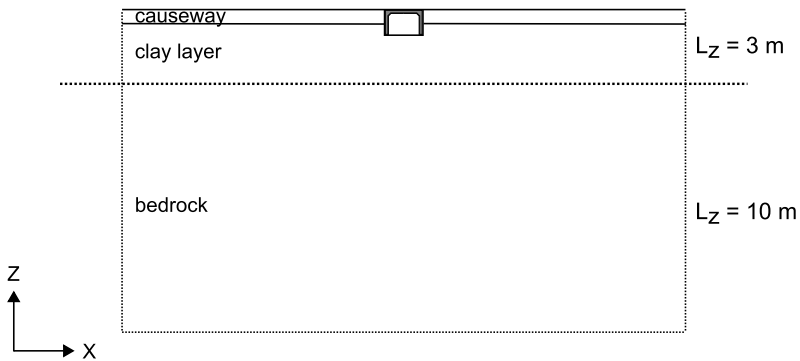


Figure 5.7: Damping ratio

5.3 Element mesh and boundary conditions

An important issue when modelling structural mechanics is how much of an object that should be part of the model. In this case the road-bridge itself plays a significant role and should obviously be part of the model. However one has to consider how much of the surrounding soil that should be incorporated in the modelling domain. Practically, the surrounding soil constitutes in some sense an infinite domain (Zienkiewicz and Taylor, 2000). One possible solution is of course to extend the model stepwise and determine when the solution is not affected and thereby consider the domain as large enough. Fortunately during the years some techniques have been developed to handle infinite modelling domains. One suitable method is to make use of so called infinite elements which in some sense is an element with an infinite extension. The main idea behind the infinite element is, in the static case, to map the geometry to a domain which is integrated towards infinity. In the dynamic case the approach is slightly different. In order to create a boundary which consumes energy and minimizes reflecting waves it is possible to prescribe artificial damping at the boundaries. This artificial damping is chosen in such manner that the reflecting waves almost vanishes. In Abaqus there are implementations of infinite elements which can create an infinite domain. In this study use was made of the element CIN3D12R. It is important to notice that even though the element is taking use of artificial damping at the boundaries there might still be some reflections of waves. Therefore the boundaries are not to be considered as completely silent, instead they are to be considered as quiet. Even though there might be some reflections at the boundaries significant advantages are given by the infinite elements since the number of elements can be reduced, thus reducing the computational cost.

Abaqus/CAE was used for generating the geometry and the element mesh. The mesh was coarser at the outer parts of the model and consequently finer closer to the centre of the model. The resolution of the element mesh is shown in the Figures 5.8-5.10 using the variables L_x , L_y and L_z which is the approximate length of an element in the denoted direction x , y and z , respectively. The dotted lines indicates the borders between regions with different element length. In Figure 5.8 the approximate element lengths in the XY-plane are shown. The approximate element lengths selected for the vertical direction are shown in Figure 5.9.

Figure 5.8: Element lengths L_x and L_y in the XY-planeFigure 5.9: Vertical element length L_z

Even though Figures 5.8-5.9 specifies the length of the elements it must be stressed that some variations occur and the values are approximate. Some differences existed around the road-bridge. The road-bridge has a more complicated geometry which resulted in a finer element mesh. An overview of the element mesh for the road-bridge is shown in Figure 5.10.

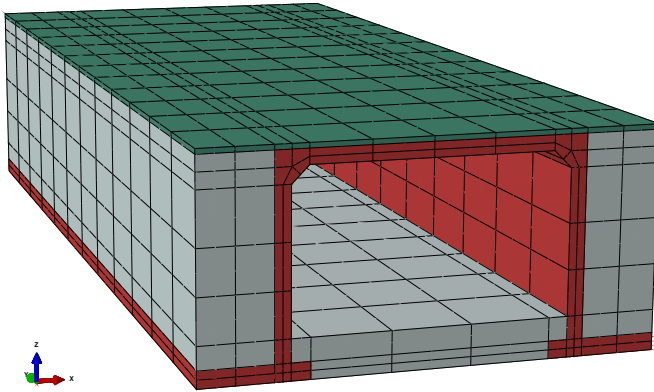


Figure 5.10: Element mesh around the road-bridge

The complete mesh for the whole model was dominated to the number and volume by the C3D20 element, which is a fully integrated isoparametric element in 3D of second order with 20 nodes. The outer boundaries are modelled with the CIN3D12R element which is an infinite element in 3D with 12 nodes and reduced integration. A problem that may arise when using infinite elements such as CIN3D12R is zero energy modes since the infinite boundaries does not provide any real boundary condition in terms of prescribed displacement. This is the explanation why the fully integrated element C3D20 had to be chosen instead of the version with reduced integration C3D20R. Table 5.1 summarizes the element mesh in terms of number of nodes and number of respective element.

| | |
|----------------|--------|
| Abaqus model | |
| no of nodes | 371090 |
| no of elements | 87036 |
| no of C3D20 | 78072 |
| no of CIN3D12R | 8964 |

Table 5.1: Mesh properties

5.4 Steady state analysis

In a steady state analysis the construction is exposed to a harmonic load. The response of the structure is calculated at different exciting frequencies i.e. a frequency sweep from 5 Hz to 50 Hz in this particular case. In Abaqus this kind of procedure was implemented in the analysis step called “Steady-state dynamics, Direct”, which calculates the complex harmonic response of the structure. The position of the load was varied and two different load cases were studied. The load cases are given the labels $f1$, $f2$ and $f3$, where $f1$ is the case where the load was placed at a centric position, $f2$ represents an excentric load case whereas $f3$ represents a load right on top of the wall of the road-bridge. The three different load positions is shown in Figure 5.11.

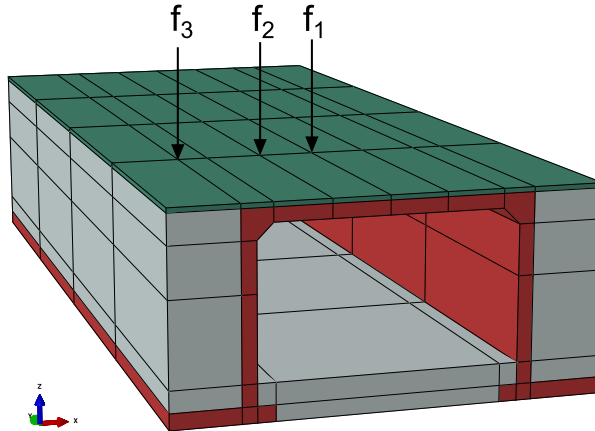


Figure 5.11: Load positions in the steady state analysis

5.5 Transient analysis

The model was also studied for a transient load case. The load case aimed at simulating the event of an over-passing vehicle. Such event is obviously an extremely complicated load case and must therefore be simplified. The load case would be possible to define by defining a model of the vehicle and connect it to the Abaqus model using contact definitions. That kind of procedures is unfortunately quite extensive. Therefore another modelling strategy was adopted in this study. The vehicle was simplified to a single axle model which is described in Cebon, 1999. The road and the road-bridge was modelled as an assembly of continuous beam elements. The complete combined model of the vehicle and the road with the road-bridge was studied in MATLAB using the CALFEM toolbox. The reaction force between the vehicle and the road was extracted from MATLAB and thereafter imported as a transient load case in Abaqus. The transient analysis can consequently be seen as a two-step calculation where a load case was created in MATLAB and subsequently transferred to the Abaqus model where the final calculation took place. The work flow of the transient analysis is shown in Figure 5.12.

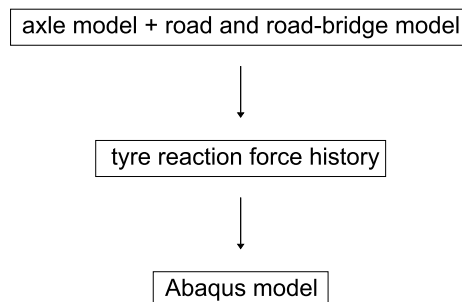


Figure 5.12: Work flow of the transient analysis

5.5.1 Axle model in CALFEM

In Cebon (1999) a simple 2-DOF-system is presented. The 2-DOF-system aims at describing an axle of a heavy vehicle, e.g. a truck. The system consists of two masses which are connected with springs and viscous dampers, see Figure 5.13. The upper and heavier mass was assumed to stand for a representative part of the truck while the lower part, consisting of a lighter mass, was assumed to represent the tyre and wheel together with the axle shaft etc. Figure 5.13 shows that an extra DOF was added to describe the ground motion, i.e. how the vertical level of the road varies.

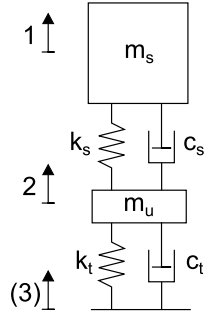


Figure 5.13: System of a heavy vehicle axle

The system shown in Figure 5.13 may be described by eq. 4.20 and the following matrices:

$$\mathbf{M} = \begin{bmatrix} m_s & 0 & 0 \\ 0 & m_u & 0 \\ 0 & 0 & 1 \end{bmatrix}$$

$$\mathbf{C} = \begin{bmatrix} c_s & -c_s & 0 \\ -c_s & c_s + c_t & -c_t \\ 0 & -c_t & c_t \end{bmatrix}$$

$$\mathbf{K} = \begin{bmatrix} k_s & -k_s & 0 \\ -k_s & k_s + k_t & -k_t \\ 0 & -k_t & k_t \end{bmatrix}$$

where the values of the mass parameters m_s and m_u are the sprung and unsprung mass respectively, the damping parameters c_s and c_t are the suspension damping and the tyre damping respectively, and k_s and k_t are the suspension stiffness and tyre stiffness respectively. The parameters are summarised in Table 5.2. It can also be noted that a symbolic mass of 1 is added to the third DOF in the mass matrix thus making the matrix non-singular.

| Mass | Damping | Stiffness |
|-------------------------|------------------------------------|----------------------------------|
| $m_s = 8900 \text{ kg}$ | $c_s = 40 \cdot 10^3 \text{ Ns/m}$ | $k_s = 2 \cdot 10^6 \text{ N}$ |
| $m_u = 1100 \text{ kg}$ | $c_u = 4 \cdot 10^3 \text{ Ns/m}$ | $k_u = 3.5 \cdot 10^6 \text{ N}$ |

Table 5.2: Parameters of the heavy vehicle axle system

One important modelling aspect of the material parameters in table 5.2 is that the parameters are given for *one* axle. It was desirable to model the

response of *one* wheel of the axle. Therefore were all parameters in the CALFEM implementation divided by two enabling a description where the reaction of *one* wheel (given the assumption or fact that the axle model have two wheels) was derived.

5.5.2 Beam model in CALFEM

Road part

The road was modelled with continuous dynamic beam elements on elastic foundation with damping i.e. so called Winkler beams (Cebon, 1999). The road-bridge was modelled with ordinary dynamic beam elements. Additional stiffness was applied to take into account effects from the road-bridge foundation and the frame construction of the road-bridge. In Figure 5.14 the mechanical model of a Winkler beam is shown.

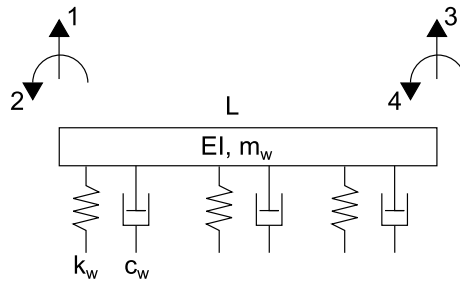


Figure 5.14: Winkler beam

The Winkler beam element is governed by the mass matrix

$$\mathbf{M} = \frac{m_w L}{420} \begin{bmatrix} 156 & 22L & 54 & -13L \\ 22L & 4L^2 & 13L & -3L^2 \\ 54 & 13L & 156 & -22L \\ -13L & -3L^2 & -22L & 4L^2 \end{bmatrix}, \quad (5.1)$$

the stiffness matrix

$$\mathbf{K} = \mathbf{K}_1 + \mathbf{K}_2$$

where \mathbf{K}_1 and \mathbf{K}_2 are the parts corresponding to bending stiffness and foundation stiffness respectively given by

$$\mathbf{K}_1 = \frac{EI}{L} \begin{bmatrix} 12/L^2 & 6/L & -12/L^2 & 6/L \\ 6/L & 4 & -6/L & 2 \\ -12/L^2 & -6/L & 12/L^2 & -6/L \\ 6/L & 2 & -6/L & 4 \end{bmatrix} \quad (5.2)$$

$$\mathbf{K}_2 = \frac{k_w L}{420} \begin{bmatrix} 156 & 22L & 54 & -13L \\ 22L & 4L^2 & 13L & -3L^2 \\ 54 & 13L & 156 & -22L \\ -13L & -3L^2 & -22L & 4L^2 \end{bmatrix}$$

and the damping matrix

$$\mathbf{C} = \frac{c_w L}{420} \begin{bmatrix} 156 & 22L & 54 & -13L \\ 22L & 4L^2 & 13L & -3L^2 \\ 54 & 13L & 156 & -22L \\ -13L & -3L^2 & -22L & 4L^2 \end{bmatrix}$$

The material parameters in the matrices are the mass per length unit m_w , the length L , the bending stiffness EI , the foundation stiffness k_w and the foundation damping c_w . It can also be noted that the expressions for the foundation stiffness matrix and the foundation damping matrix are analogous. The modelling assumptions and selection of the parameters defining mass, stiffness and damping properties for the road part of the model were made according to the following:

- The cross section was assumed to have the width $b = 1$ m and the height $h = 0.15$ m, see Figure 5.15. The cross section was assumed to consist of the asphalt material defined in Table 2.1. The bending stiffness EI and the mass per length unit m was calculated using the given assumption of the cross section.

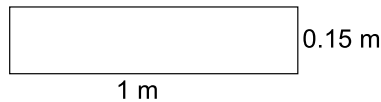


Figure 5.15: Asphalt/Winkler beam cross section

- The foundation stiffness k_t and the foundation damping c_t were given values such that the vertical displacement of the road, when the wheel of the axle passed at a speed of 30 m/s, was 15 mm.

The above assumptions leads to values of the parameters which is in the same magnitude as those given by Cebon (1999). The main difference are the values of k_t and c_t . The proposed values by Cebon (1999) gives a smaller vertical displacement around 0.5 mm.

Road-bridge part

The road-bridge was modelled using ordinary dynamic beam elements (Austrell et al., 2004). In Figure 5.16 the mechanical model of the dynamic beam element is shown.

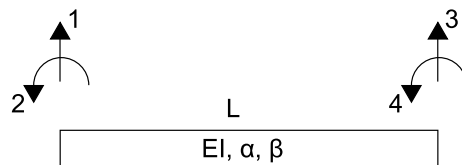


Figure 5.16: Dynamic beam element

The mass matrix \mathbf{M} and the stiffness matrix \mathbf{K} for the dynamic beam element was defined according eq. 5.1 and eq. 5.2, respectively. The damping

matrix \mathbf{C} was created using Rayleigh damping given by eq. 4.16. The modelling assumptions and selection of the parameters defining mass, stiffness and damping properties for the road-bridge part of the model were made according to following:

- The cross section was assumed to have the width $b = 2$ m and the height $h = 0.6$ m, see Figure 5.17. The reason why b was increased to 2 m (compared to the road part where $b = 1$ m) was the assumption that the road-bridge also partially can be regarded as a plate, thus increasing the effective width of the modelled beam. The cross section was assumed to consist of the concrete material defined in Table 2.1. The bending stiffness EI and the mass per length unit m was calculated using the above given assumption of the cross section.

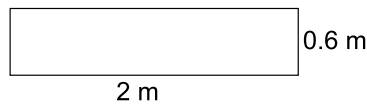


Figure 5.17: Cross section road-bridge beam

- The damping was modelled with Rayleigh damping where the Rayleigh parameters α and β were chosen according to Table 2.1.
- Extra vertical stiffness and rotational stiffness was added to the degrees of freedom at the start and at the end of the road-bridge part of the model in order to take into account stiffening effects from the road-bridge walls. The values of the extra vertical and rotational stiffness were calibrated to give approximately the same displacement magnitude and shape as the Abaqus model.

Complete beam model

Two road parts and one road-bridge part, defined according to the previous text, were connected to each other and thereby constituted a complete beam model, on which the axle model was run. An overview of the complete beam model is shown in Figure 5.18.

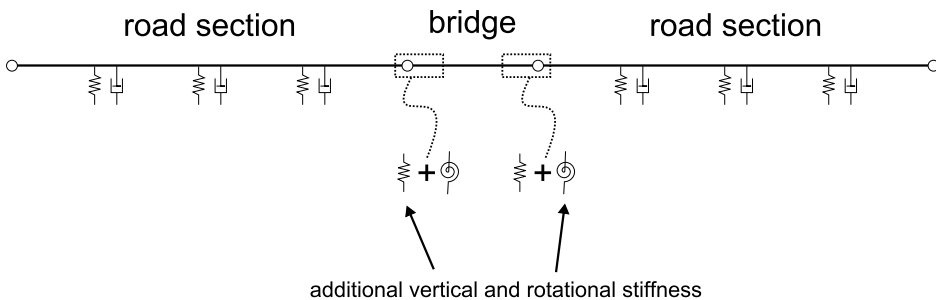


Figure 5.18: Overview of the complete beam model

5.5.3 Connection of axle model and beam model

The axle model and the road model were connected to each other using the conditions where the reaction force from the tyre was transferred to the road and that the tyre followed the variation of the displacement of the road. Essentially, the wheel was run over the road and the reaction force between the tyre and the road was studied. The variation of the tyre reaction force was of special interest since it formed the basis for the transient load. The motion of the axle along the road model was done by stepwise movement from one node to next node along the road beams at a speed of 30 m/s. This speed is higher than the legal maximum speed for a heavy vehicle in Sweden. However it is still a speed that may not be unlikely for a heavy vehicle. Along the driving path, the response of the axle model and the beam model was evaluated using a time integration scheme based on the theory described in section 4.2.4. The time integration parameters were given the values $\alpha = \frac{1}{4}$ and $\beta = \frac{1}{2}$, which corresponds to the average acceleration (trapezoidal) rule (Austrell et al., 2004). The basic idea of the solution procedure adopted is summarised in the following scheme:

0. Create initial conditions
1. Calculate the vertical displacement of the beam at the tyre position, u_{beam}
2. Calculate the change of vertical displacement Δu_{beam}
3. Update vertical position of the tyre $u_{tyre} = u_{tyre} + \Delta u_{beam}$
4. Calculate reaction of the axle model from u_{tyre}
5. Move the tyre to next node
6. Return to (1)

The iteration scheme is expressed graphically in Figure 5.19.

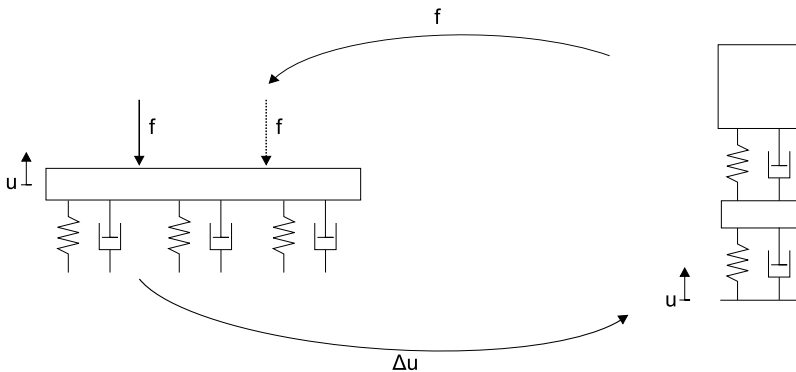


Figure 5.19: Illustration of iteration scheme

The above code is in some sense an explicit scheme where the next state is directly calculated from the previous one, without ensuring that equilibrium is reached between the two partial models. Fortunately one can show that if the time step, i.e. the length of the beam elements in this case, is sufficiently small

the solution converges towards the exact solution. Practically the length of the beam elements and thereby the time step were decreased until a stable solution, where the reaction force followed a smooth curve, was achieved. An example plot of the result from an analysis is shown in Figure 5.20. The solid lower line shows the static deflection along the road for a unit point load whereas the upper solid line shows the variation of the reaction force between the tyre and the road the road. Text notes indicate the initial/static, maximum and minimum reaction force. The axle model was run from left to right.

From Figure 5.20 it can be noted that the reaction force may be divided into two parts; one static load (which is equal to the initial/static load 48.996 kN) and one dynamic load which is varying when the axles passes the bridge. The static load will, of course, generate a displacement. It is possible to show that the static load is moving under the critical speed for generating vibrations in the ground, i.e. the static load may be considered as a quasi-static load. Therefore, it is desirable to only study the dynamic part of the load, i.e. the variation of the load. The dynamic part of the load is found by subtracting the mean value, i.e. the static load, from the total reaction force. The obtained dynamic load is shown in Figure 5.21.

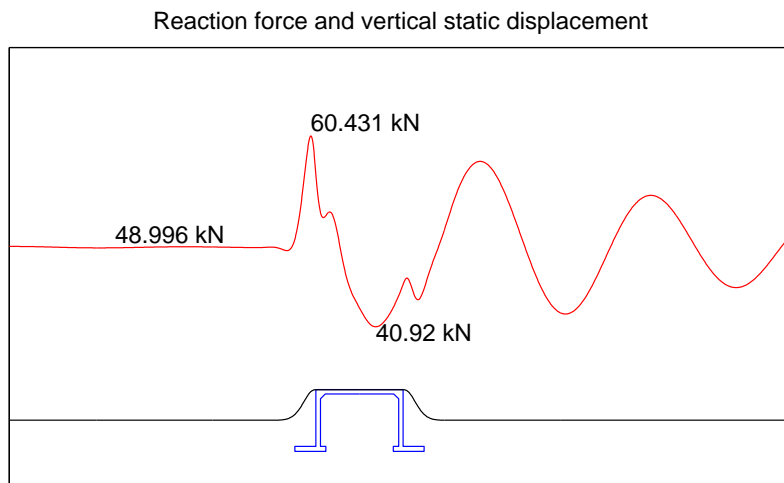


Figure 5.20: Reaction force(the upper line) and vertical static displacement(the lower line)

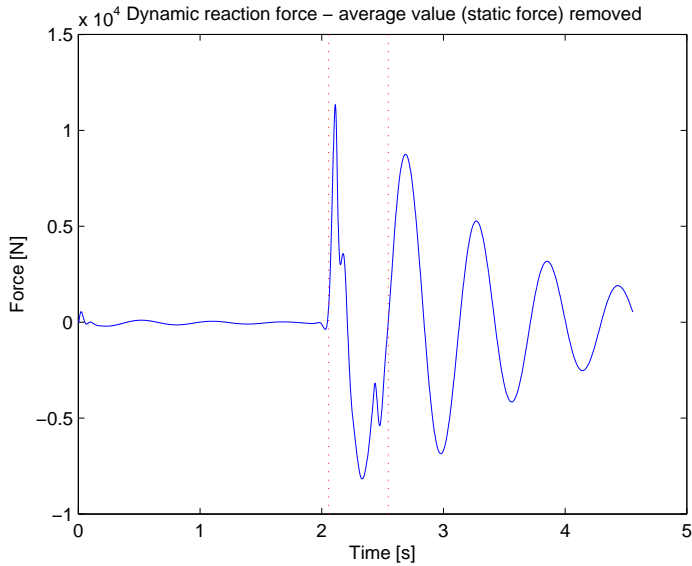


Figure 5.21: Dynamic reaction force between the tyre and the road

Horizontal component of load

The vertical reaction force of the tyre was studied and the dynamic variation of the load was plotted in Figure 5.21. A possible horizontal component was also studied. However, it was concluded that the horizontal component of the load could be neglected. The following text describes the procedure and the result from the calculation of the horizontal component of the load.

In general the reaction force in the horizontal direction must be equal to zero since there are no force generating phenomena such as gravity etc. However, it is not far away to think that a change of the geometry of the road can create a horizontal reaction force. In order to study a possible horizontal component of the tyre reaction force a model which represented the vehicle was established, see Figure 5.22.

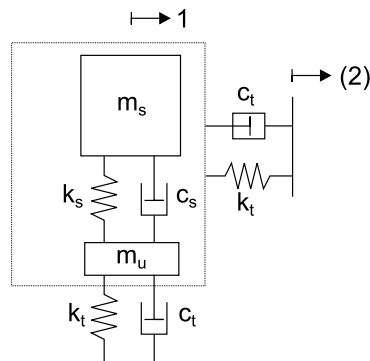


Figure 5.22: Suggestion of horizontal vehicle model

The main assumption of the horizontal force model was that only the tyre acts as a spring and damper, i.e. the upper greater mass was assumed to make a rigid connection to the tyre without any spring and damping. Consequently a system was defined with one DOF describing the motion of the vehicle and one DOF describing the ground motion. In the axle model, and all spring and damper models as well, a change of the distance between the point which connects the spring and damper is a source of generating a reaction force. A force may in this case be created if a difference in speed exist between the mass and the the ground motion DOF. This was likely to occur when the vehicle had to pass the road-bridge. As seen in Figure 5.20, when looking at the static deflection, the road-bridge in some sense acts as a bump in the driveway. A possible solution of handling the mechanics of the situation when the vehicle had to pass the bump was to assume that the total mass was forced to continue with a constant horizontal speed. It was also assumed that the *ground motion* followed the shape of the static deflection in Figure 5.20 and had a speed which was constant at a view *parallel to the ground*. Since the driving path was not parallel to the horizontal axis when the vehicle passed the bump a difference in speed between the mass and the ground was generated. This difference in speed was calculated and thereafter studied in a case when the horizontal ground motion was slower than the horizontal motion of the total mass. The result of the case when the vehicle reached the left part of the road-bridge and was forced to to climb up the bump is shown in Figure 5.23.

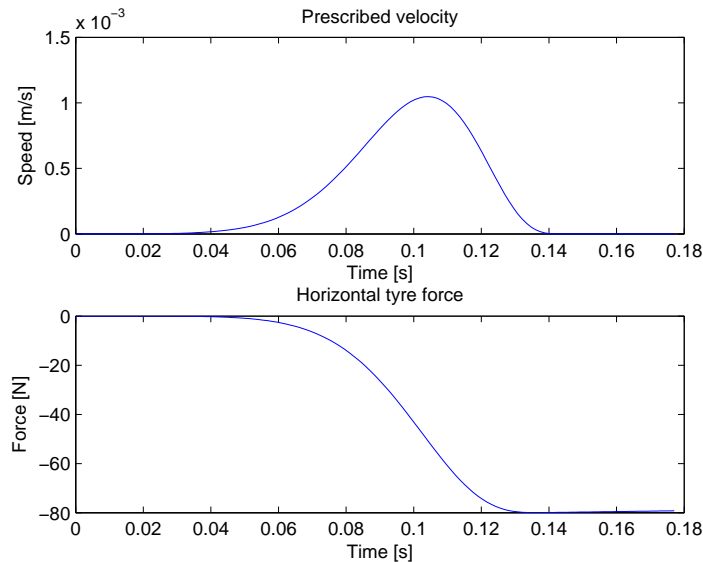


Figure 5.23: Relative speed and horizontal force

In the upper plot of Figure 5.23 the total mass horizontal speed relative to the ground motions horizontal speed is shown. In the lower plot of Figure 5.23 the horizontal reaction force is shown. One can notice that it is a quasi-static process where no dynamic oscillations are involved. This method of handling the case of passing the road-bridge does not give an answer regarding how the horizontal force is released. Fortunately, in this case, that was not a problem since the magnitude of the load was very small compared to the vertical magnitude. This difference in magnitude served as the main argument to ignore the horizontal component of the load.

5.5.4 Defining transient load case in Abaqus

The load history of the dynamic tyre force variation along the road-bridge was defined in the previous section. This time history was transferred to Abaqus for further analysis. However, some manipulations of the load history were needed in order to define it in Abaqus. Initially, a selection was made of which time of the total load history that were of interest. An extraction was made during the marked interval as shown in Figure 5.21. The marked interval corresponds to the time history where the axle is passing the road-bridge. One could insist on that the whole dynamic load history should be part of the analysis. This was not done given the following two reasons: firstly, the dynamic part of the load history was initially zero and thereby not generating any load, secondly, the influence of the road-bridge was the main interest in this analysis and the load was assumed to not have crucial influence on the road-bridge after it has passed it.

As shown in Figure 5.21 it is possible to define the load history as a function of time, i.e. the load history f can be written as $f = f(t)$. Point loads were created in the Abaqus model at nine discrete points, see Figure 5.24.

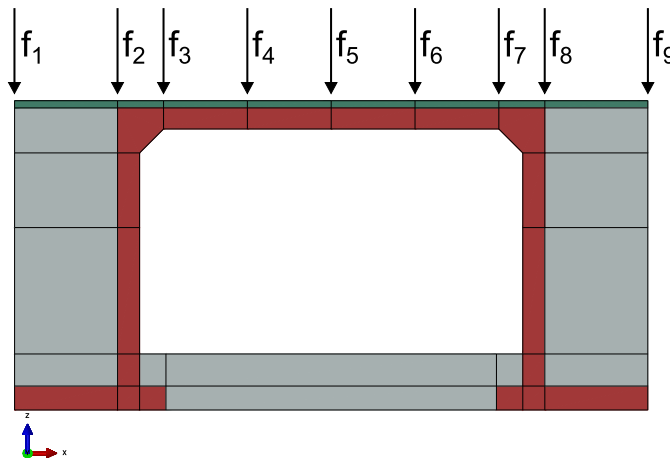


Figure 5.24: Point loads in Abaqus

Fortunately it was possible to define how the point loads in Abaqus varied with time. The next step was thereby to determine how the value of the point load should change during time. In order to create the load history for each nine discrete points advantage was taken from the concept of shape functions (Ottosen and Petersson, 1992). A shape function $N_i = N_i(t)$ was defined for each discrete point $i = 1, 2, \dots, 9$ during the time of interest t . One could therefore derive an expression for the load history at each discrete point by using the following relation:

$$f_i(t) = N_i(t)f(t); \quad i = 1, 2, \dots, 9.$$

In Figure 5.25 an example of the shape function N_2, N_3 and the local load history for load point $i = 2, 3$ are shown. One can notice that the shape function varies linearly and takes the value 1 when the axle passes the point and takes the value 0 when the axle is at the other points. These properties are common for all shape functions. It is also evident that

$$\sum_{i=1}^9 N_i(t) = 1$$

holds for all values of t . When the local load histories had been created it was possible to insert them into the Abaqus model as point loads which varied according to the previously defined functions of time. Basically one can say that two separate wheel paths were created where each path corresponded to one track of the axle. A graphic illustration of the load case in Abaqus is shown in Figure 5.26.

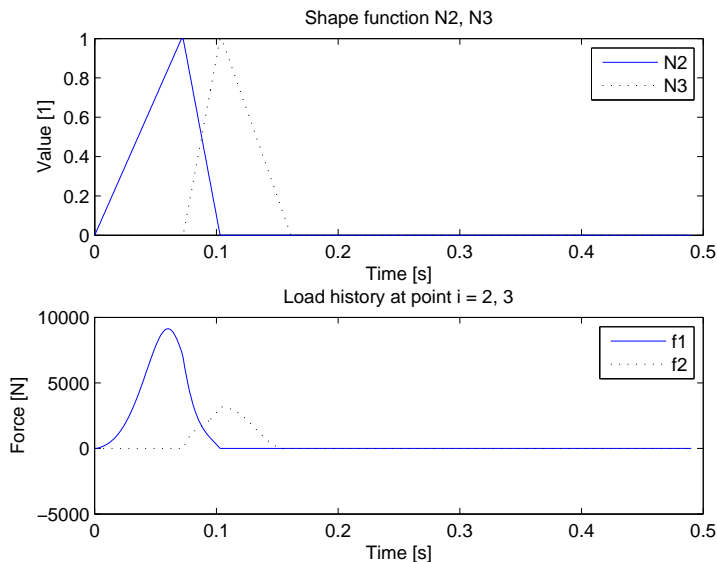


Figure 5.25: Example of shape functions and local load histories

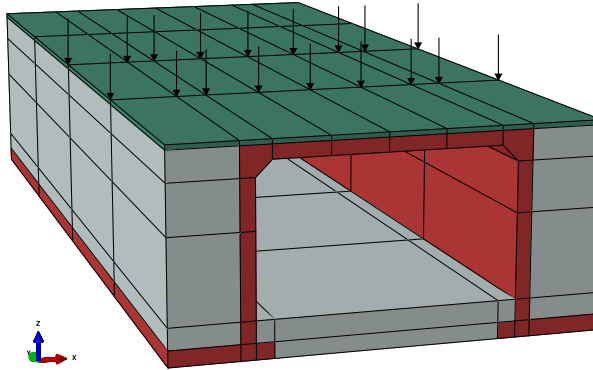


Figure 5.26: Point loads in Abaqus

Finally the analysis was performed by Abaqus using a time integration procedure defined as a “Dynamic, Implicit” step. The time integration procedure was chosen to use a fixed step time with $\Delta t = 0.005$ s which gives a resolution in the frequency domain of $f = \frac{1}{2} \frac{1}{0.005} = 100$ Hz. As shown in Figure 5.7 the damping increases with higher frequencies and thereby the response of structure decreases, which also have been showed in the displacement spectrograms of the measurements.

Chapter 6

Modelling results

In this chapter the results obtained from the modelling are presented and discussed.

6.1 Definition of result points

In the following sections the results from the modelling are presented. The results describe the response at specific points. These points were chosen to be identical in position to the measurement points discussed in Chapter 3. In Chapter 3, measurements where passages of vehicles from which were southbound and northbound were presented. It is not necessary to perform calculations for both southbound and a northbound load-cases, since a possibility to use the symmetry of the model exist. This symmetric property is shown in Figure 6.1.

In addition to the measurement points on the road-bridge, results from a point corresponding to the seismometer station labelled “Pos new” were extracted. In Figure 6.2 the relative position of the seismometer station to the road-bridge is shown. The symmetric property of the modelling domain was also taken into account to extract result data from southbound as well as northbound passages.

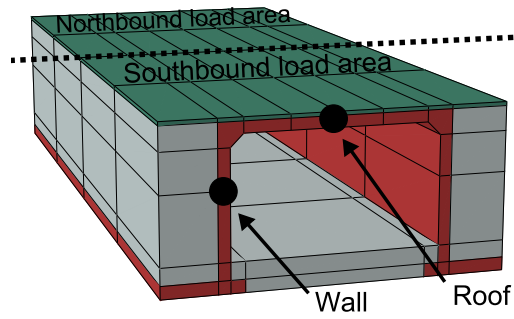


Figure 6.1: Locations of measurement points Roof and Wall in the modelling domain

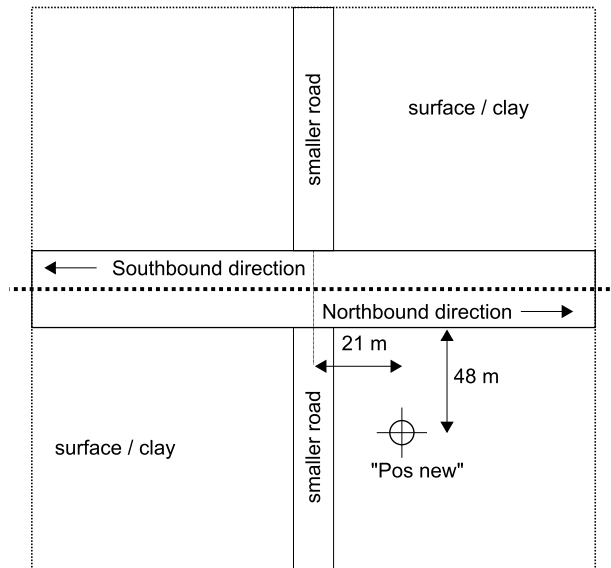


Figure 6.2: Location of seismometer station "Pos new"

6.2 Steady state analysis

In the Figure 6.3-6.4 the displacement magnitude response in the U1- and U3-direction for the steady-state analysis at the corresponding measurement points at the roof and at the wall for the load-cases $f1$, $f2$ and $f3$ (see Figure 5.11) are shown. In the legend of the plots *northbound* and *southbound* have been abbreviated to *NB* and *SB*, respectively. In Figure 6.5 the obtained result for the U2-direction is presented.

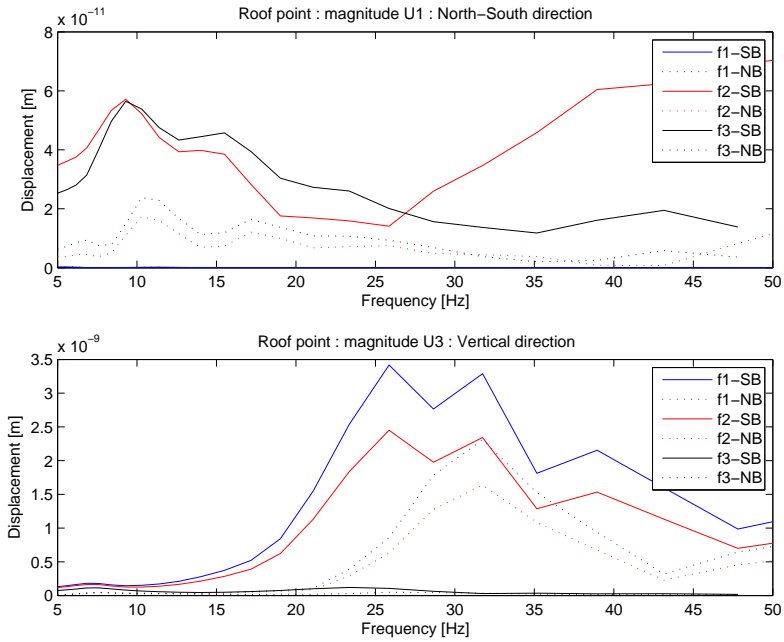


Figure 6.3: Displacement magnitude response at measurement point Roof

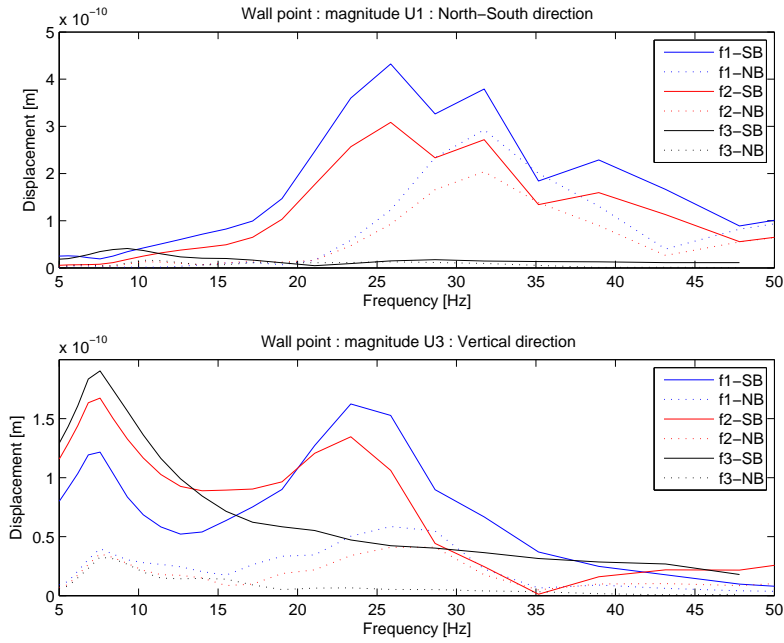


Figure 6.4: Displacement magnitude response at measurement point Wall

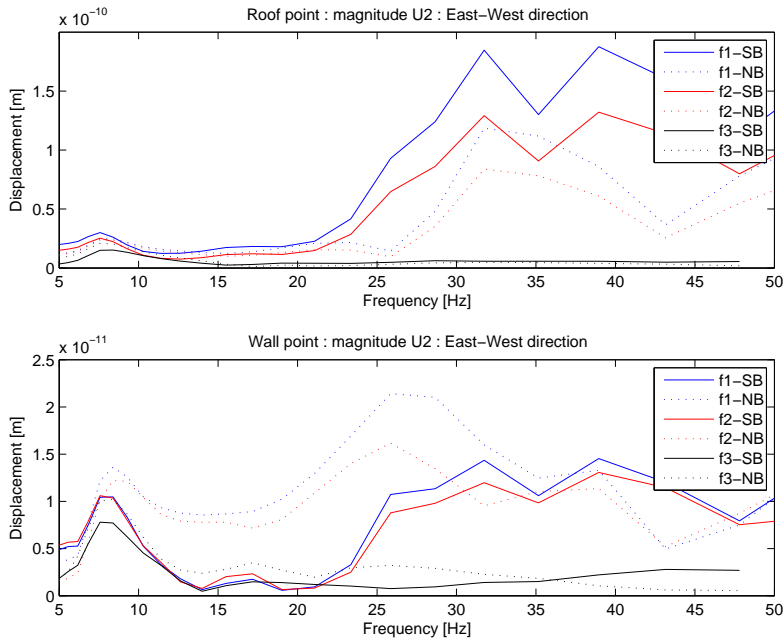


Figure 6.5: Displacement magnitude response in U2-direction at measurement point Roof and Wall

It can be noted that the response in the U2-direction for the wall is in a considerably less magnitude compared to the U1- and U3-direction. This serves as an argument to why the focus is directed towards the U1- and U3 directions further on when discussing the response of the road-bridge.

Another information that was studied in the result from the steady state analysis was the shape of the structural movement at the different exciting frequencies. An example of a plot of the movement at the exciting frequency 11 Hz is shown in Figure 6.6.

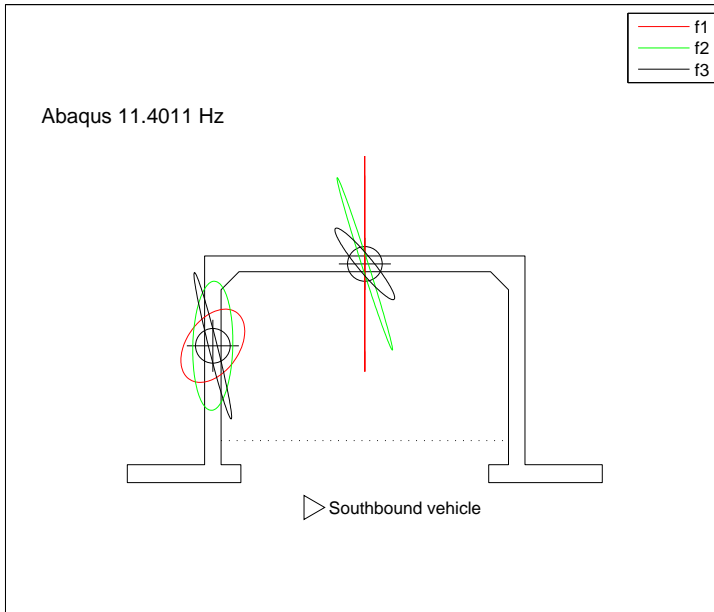


Figure 6.6: Structural movement at steady state response

6.3 Transient analysis

6.3.1 Response of road-bridge

The structural response to the transient load was evaluated and in the Figures 6.7-6.10 the time histories of displacement for positions in the model which corresponds to the locations of the measurement points in Chapter 3 are shown. In all figures it is clearly visible that the model is a highly damped system. In general a significant displacement response is only present as long as the loading is present, i.e. during an approximately time interval of 0.5 s. In the Figures 6.7-6.10 the frequency content of the time histories also are shown.

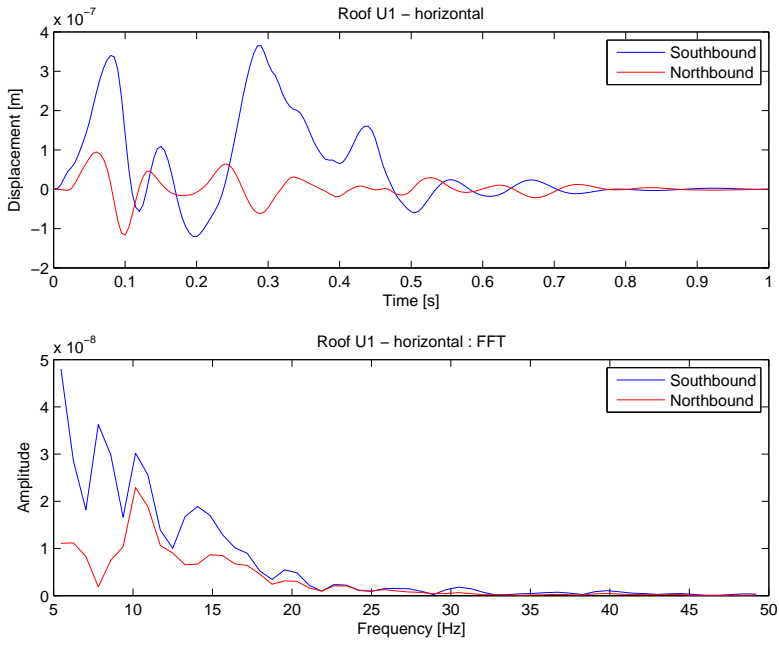


Figure 6.7: Displacement time history and frequency content Roof U1 - horizontal

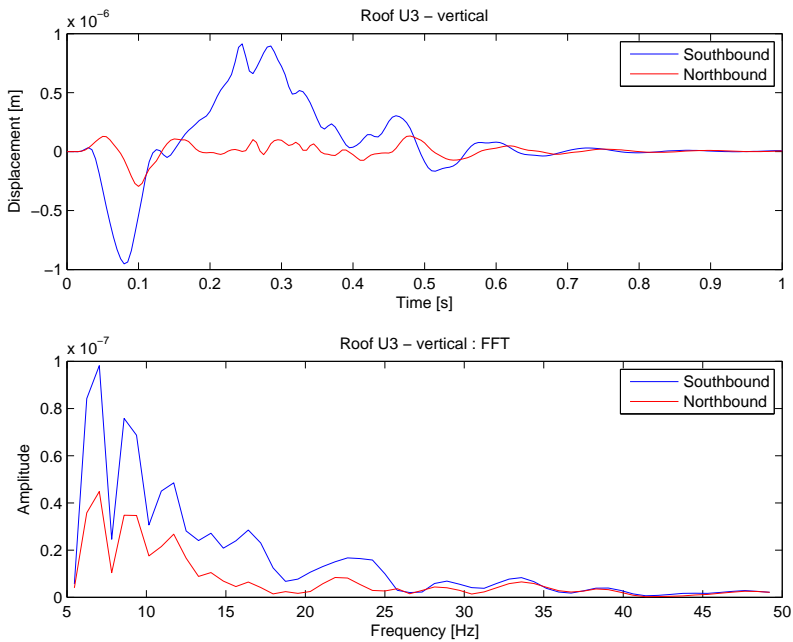


Figure 6.8: Displacement time history and frequency content Roof U3 - vertical

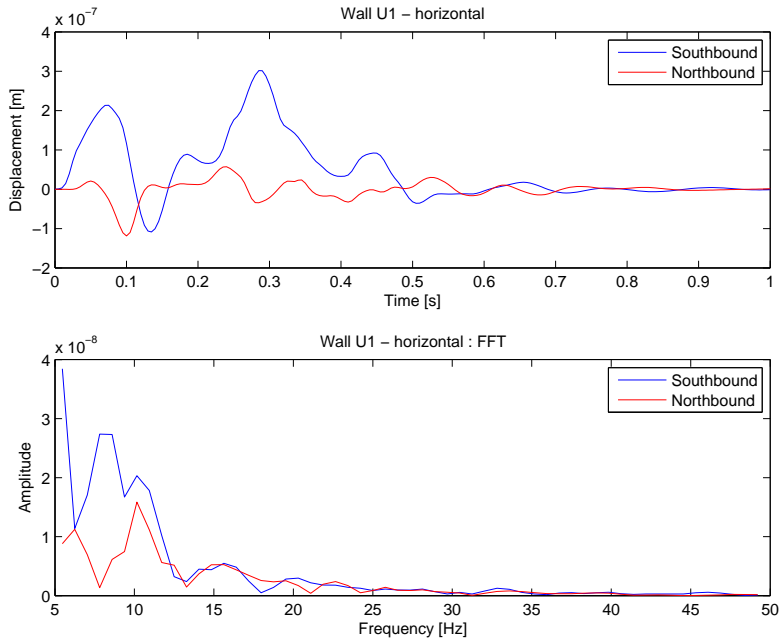


Figure 6.9: Displacement time history and frequency content Wall U1 - horizontal

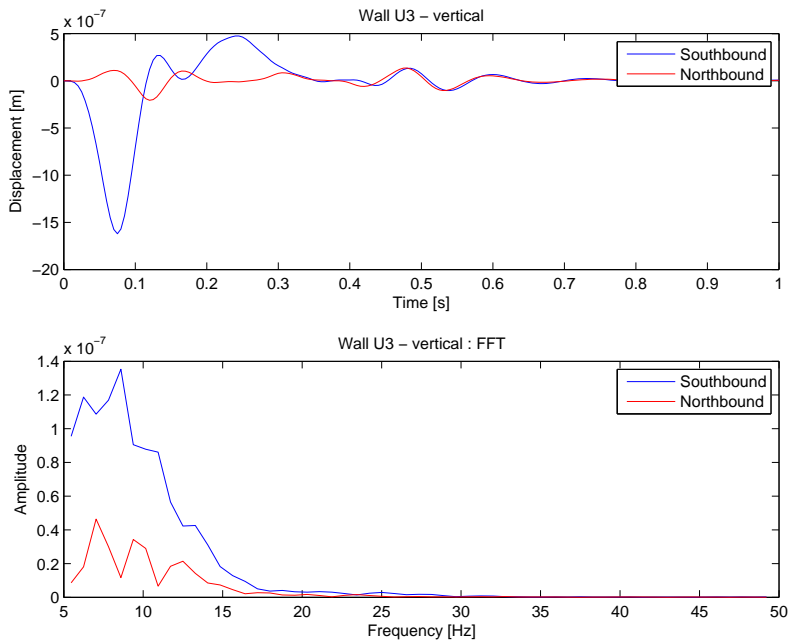


Figure 6.10: Displacement time history and frequency content Wall U3 - vertical

The results U2-direction are not presented since the maximum amplitude of U1 for the roof point is about a four times greater than the corresponding maximum amplitude of U2. The same comparison for the wall point yield a factor of a ten. Furthermore, measurements were not performed in the U2-direction for the road-bridge. Thereby no data exist which can be used to verify the modelling results.

6.3.2 Response of soil

It is of interest to give a hint on how the displacement of the soil varies due to the transient load. The time histories of the displacement were extracted for a point in the model which corresponds to the position of the seismometer labelled as “Pos new”. In Figures 6.11-6.13 the displacement time histories and frequency content for the U1, U2 and U3-direction are shown. RMS-values for the displacement histories have also been included in the plot of displacement time history. The RMS-values were calculated using a “window” with a length of one second. The magnitude of the maximum RMS-values are also displayed in the figures.

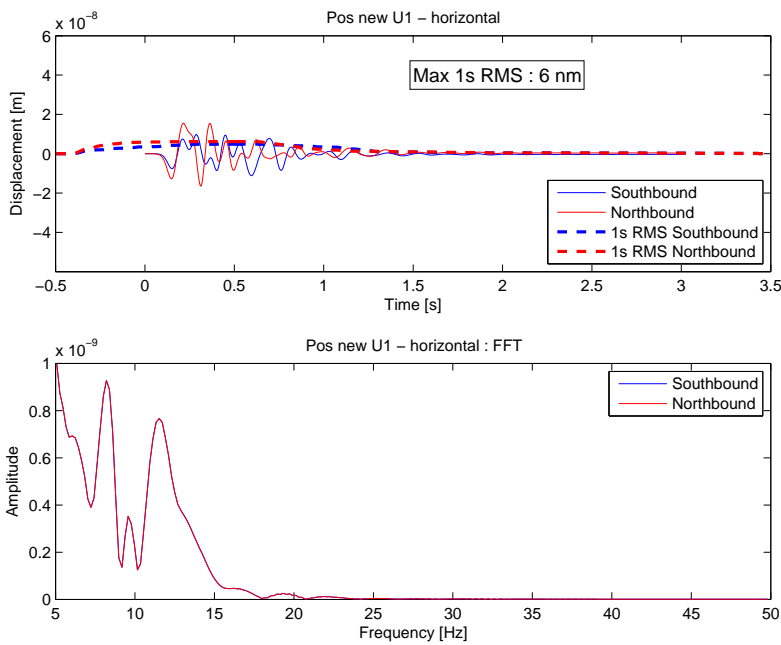


Figure 6.11: Displacement time history and frequency content U1

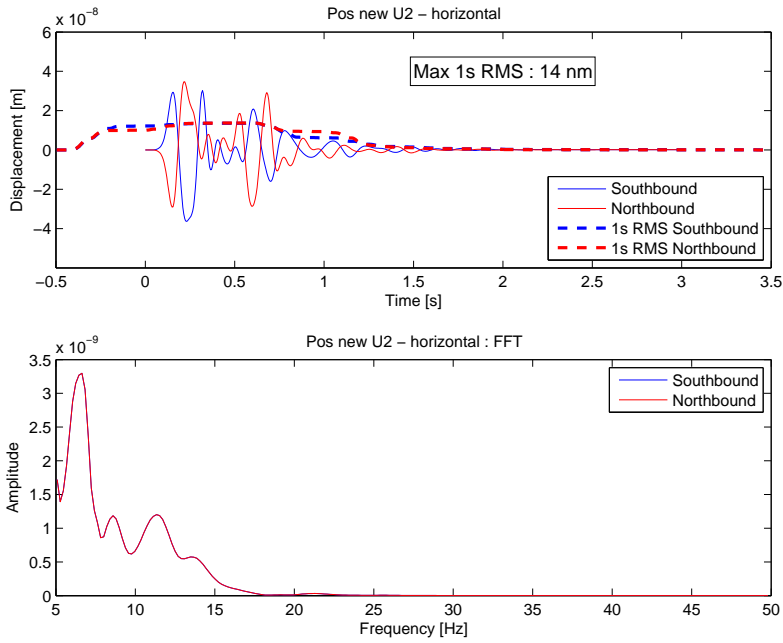


Figure 6.12: Displacement time history and frequency content U2

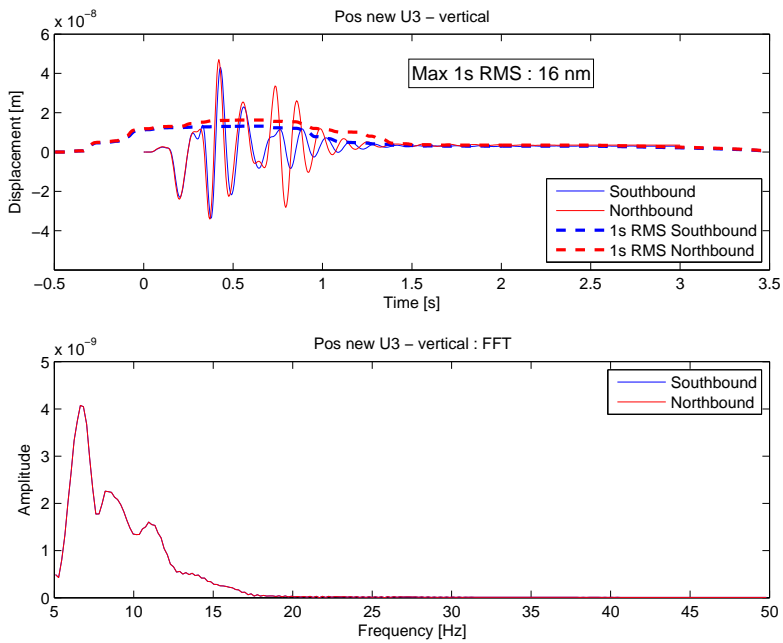


Figure 6.13: Displacement time history and frequency content U3

One observation from the Figures 6.11-6.13 is that the responses for the southbound and the northbound vehicles were approximately the same in terms of amplitude. The main difference was a phase shift.

Chapter 7

Comparison of experimental and numerical results

This chapter presents a comparison between the modelling results and the measurement data.

7.1 Steady state analysis

In section 3.2.1 a presentation of the frequency content of the measured data was given. In section 6.2 the result from the steady-state analysis was presented. To make a comparison between the measured response and the calculated values from the steady-state analysis a normalization of the values from the modelling results were made. The frequency response curves from the modelling was individually normalized to have a maximum value of unit one. The normalization procedure enabled a possibility to compare the shape of the response rather than the difference in magnitude between the different load-cases. The normalized frequency response curves from the modelling results were compared to the measured normalized average PSD from the spectrograms. In Figure 7.1-7.2 comparisons between data from the measurement and results from the modelling are shown.

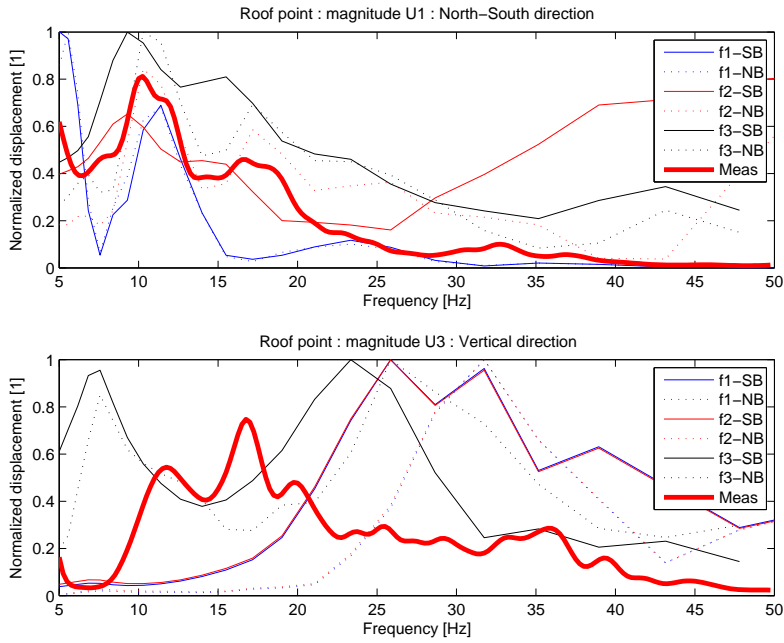


Figure 7.1: Comparison for the Roof point

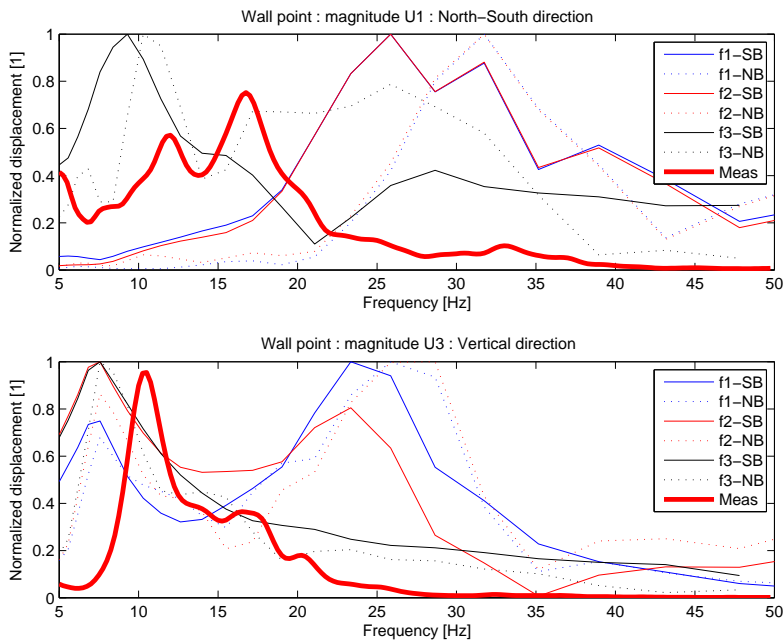


Figure 7.2: Comparison for the Wall point

The best conformity between the calculated response and the measured response was found in the U1-direction for the roof. A minor similarity between the calculated response and the measured response was seen in the U3-direction for the wall. Otherwise there were more differences than similarities. The mismatches were in general more articulated in the higher frequencies. It was concluded that the real load case of a passage of a vehicle is much more complicated than a simple point load at a fixed point.

Another result from the steady state analysis which was compared with measurement data was the shape of the movement. In Figure 6.6 the movements for the calculated responses at the frequency 11 Hz are shown. It was possible to create analogous plots for the measured movement at the same frequency as well. It has also been shown in Figure 3.15 that an in some sense articulated response in the measurements was present around the frequency 11 Hz. It was therefore of interest to study a comparison of the calculated and the measured movement at that specific frequency in a combined plot. An example of such plot is shown in Figure 7.3. In Figure 7.3 the movement for the southbound passage *p18* is presented. The measured movement was extracted from the complex amplitude from the short time FFT which was calculated when generating the spectrogram for the time point at the passage.

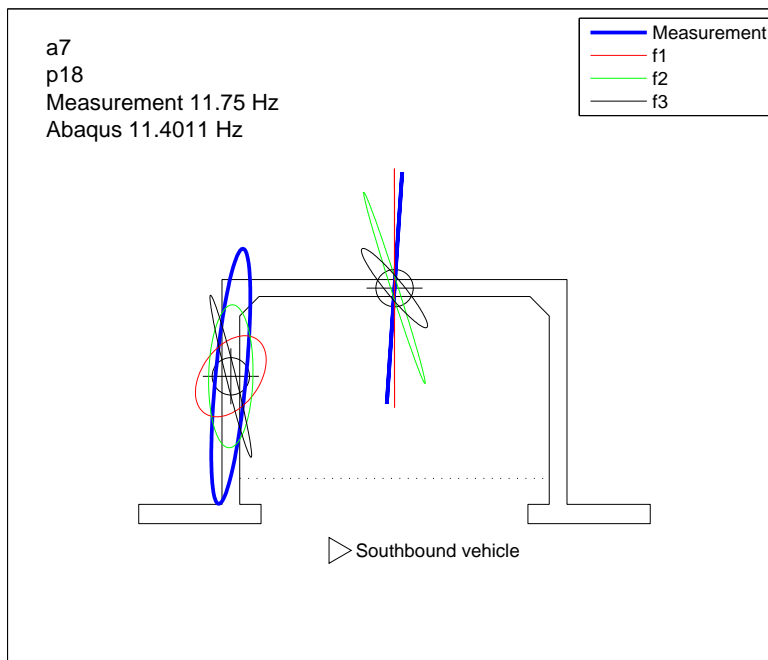


Figure 7.3: Comparison of movement for southbound passage *p18* at frequency 11 Hz



Figure 7.4: Vehicle in southbound passage *p19*

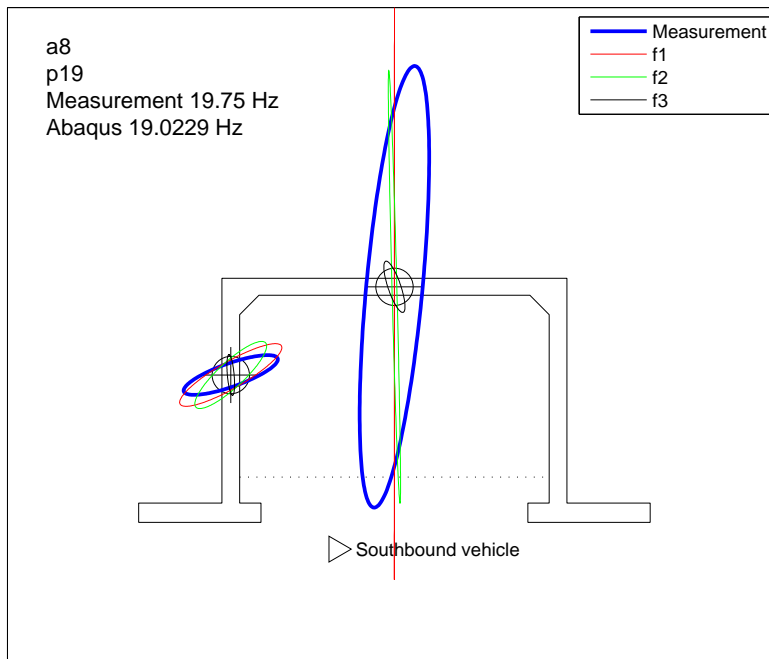


Figure 7.5: Movement of southbound passage *p19* at frequency around 20 Hz

It was also possible to study the movement at other frequencies as well. The vehicle in the passage *p19* is shown in Figure 7.4 and the corresponding movement of the road-bridge at the frequency of 20 Hz is shown in Figure 7.5.

The calculated movements from the steady state analysis was based on a loading situation defined by a simple point load at three different locations (see Figure 5.11. From the plotted movements in Figure 7.3 and Figure 7.5 it was experienced that the load case labelled f^3 seemed to have the least conformity with the measured response. It was concluded that the response of the road-bridge in general is a complex combination of many different load positions, frequencies and magnitudes at the same time. The results from the comparison were useful in terms of validating the model. The fact that the movement of the calculated response and the measured response at some frequencies agreed fairly well served as an indication that the model could be used for predicting the structural behavior of the real road-bridge.

7.2 Transient analysis

In Section 3.2.2 the measurement data of the wall- and roof point was presented. In section 6.3.1 the corresponding modelling result was presented. It has previously been mentioned that the load and the displacement may be divided into one quasi-static part and one dynamic part. The frequency content of the quasi-static movement itself is too low to create any vibrations that might disturb the MAX-lab facility. The main interest was therefore to study the dynamic part of the movement which have been measured. No breakdown of the result from the modelling was needed since the transient load-case only consisted of the dynamic part of the total load. To study the dynamic part of the measured movement the quasi-static part was removed. The removal of the quasi-static part was made by applying a highpass filter to the measured signal. The characteristics of the highpass equiripple filter which was used is shown in Figure 7.6.

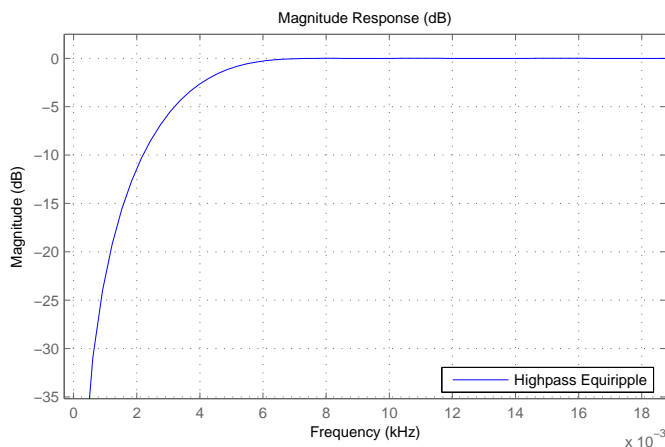


Figure 7.6: Highpass filter characteristics

The movement for the measurement points at the roof and wall at the road-bridge for the southbound passage p18 was studied. The passage p18 is the same passage that was presented in Section 3.2.2. In the Figures 7.7-7.8 the movement of the roof and the movement of the wall are shown. The left side of the two figures contains the total movement whereas the right side of the figures contains the highpass filtered time histories of the displacements. The filtered plots still contain parts of the low frequent quasi-static movement since it is in general not possible to design a perfect filter. The results from the transient analysis in Abaqus with its corresponding limits for the maximum displacements have also been inserted into the plots of the dynamic part of the movement.

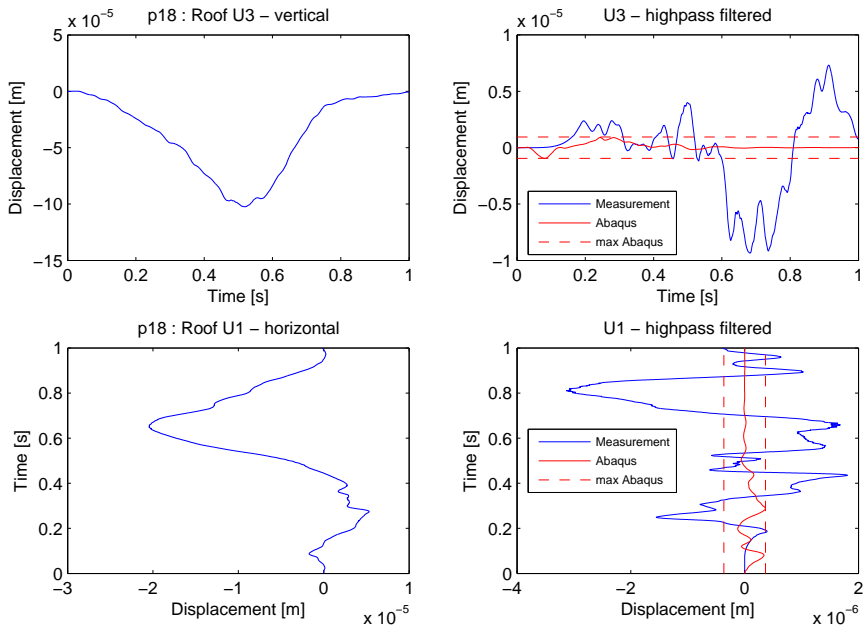


Figure 7.7: Total and dynamic movement of measurement point Roof during the southbound passage p18.

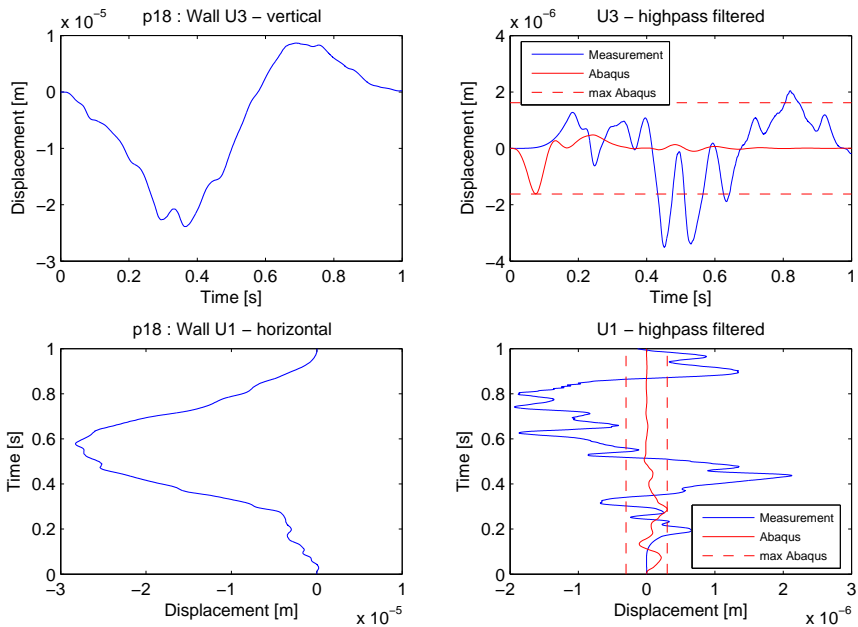


Figure 7.8: Total and dynamic movement of measurement point Wall during the southbound passage p18.

In Section 3.2.2 a presentation of a northbound passages labelled p32 have been made. It was possible to apply a highpass filter to the measured signal of the northbound passage p32 as well. The displacement time histories of the measurement points at the road-bridge is shown in Figure 7.9-7.10

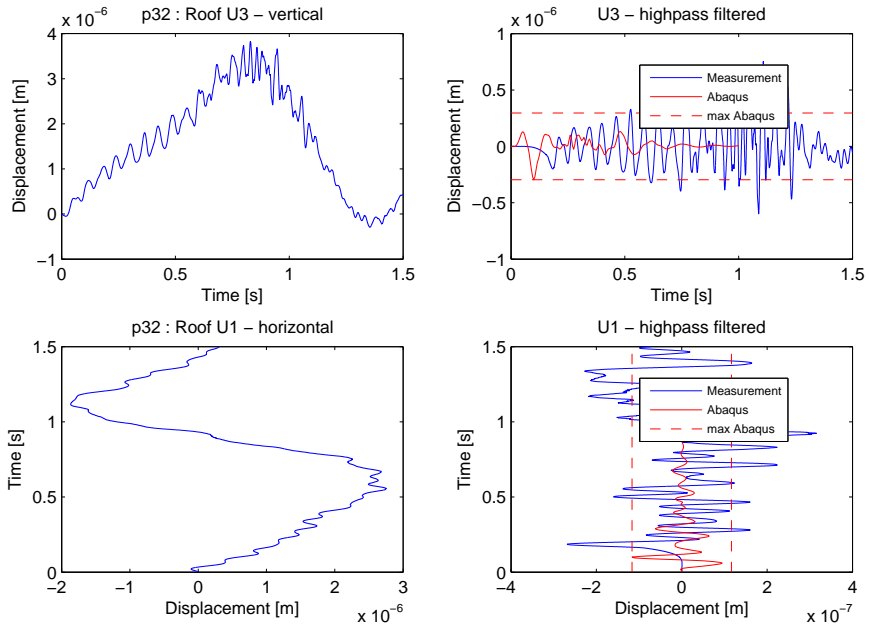


Figure 7.9: Total and dynamic movement of measurement point Roof during the northbound passage p32.

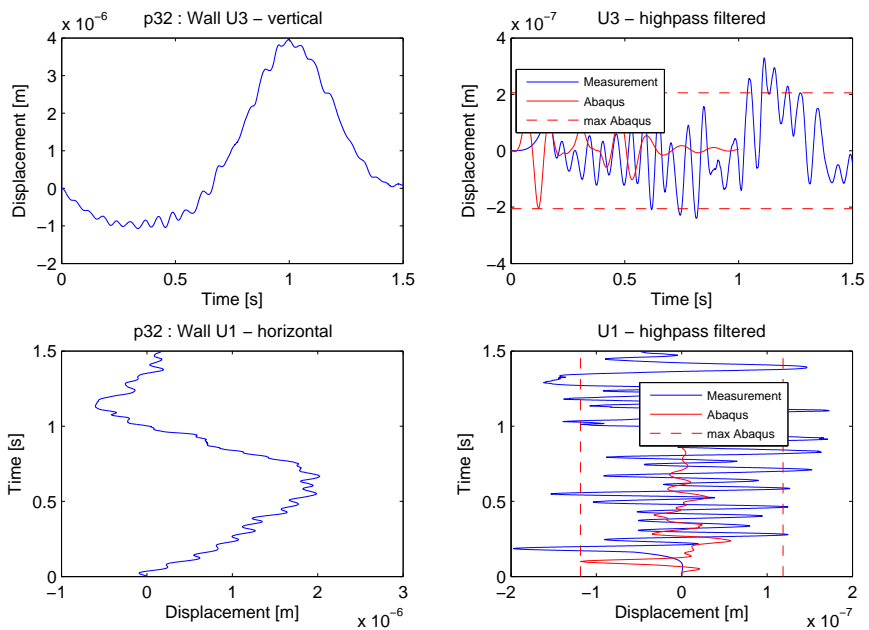


Figure 7.10: Total and dynamic movement of measurement point Wall during the northbound passage p32.

A better conformity was in general received for the measurement point Wall compared to the measurement point Roof. A similar relation was also found when a comparison was made between short and longer vehicles. Short vehicles seemed to give a better conformity rather than longer vehicles. It was impossible to determine the exact weight of the vehicles in the passages, however it is reasonable to assume that that a 24 meter long truck with a trailer constituted a greater mass than an ordinary shorter truck. An example of a typical long and probably heavy truck with a trailer is shown in Figure 7.11. The displacement time histories of the measurement points are shown in Figure 7.12-7.13.



Figure 7.11: Truck in southbound passage p16

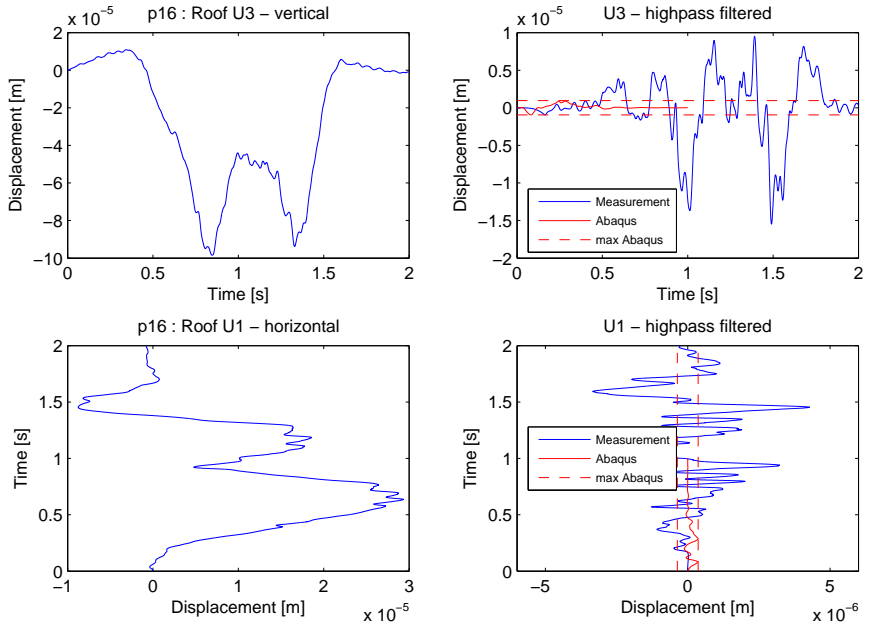


Figure 7.12: Total and dynamic movement of measurement point Roof during the southbound passage p16.

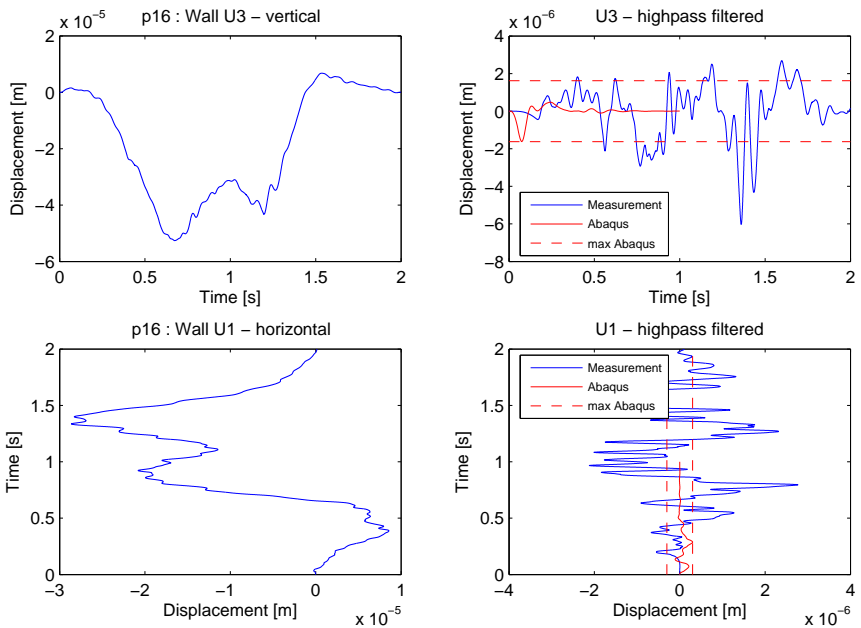


Figure 7.13: Total and dynamic movement of measurement point Wall during the southbound passage p16.

By studying the total movement in southbound passage p16 it was possible to conclude that the vehicle in p16 was heavier than the vehicle in the southbound passage p18. Consequently, a greater mass lead to a greater quasi-static displacement which furthermore had a greater impact on the highpass-filtered signal since it was not possible to *completely* remove all low frequencies. Therefore it was likely that the conformity seemed to be less good when a large quasi-static displacement was present. The fact that the trend of dynamic movement often tended to follow the total movement also served as an indication of a present influence of the quasi-static movement in the studied dynamic movement. It was concluded that the best *experienced* conformity between modelling results and measured data were received when the quasi-static movement had its smallest value. In other words, the best *experienced* conformity was received during northbound passages.

Another property which was possible to compare between modelling results and measured data was the time duration when the displacement histories had a significant response. It was obvious that the measurements in all cases showed a response with a duration that was longer than the corresponding modelling result. This was certainly not surprising since the modelling result was based on a load-case which simulated only one single axle passage whereas the measurement data showed the response for a multiple axle passage, i.e. a passage of a vehicle. A load-case including multiple axes would have lead to a better conformity regarding the time duration.

The displacement historis as well as the frequency content of the response to the transient load are presented in Figure 6.7-6.10. A comparison have previously been made in terms of displacement amplitudes and time duration. It was also possible to compare the frequency content as well. In Figure 7.14-7.15 the normalized frequency content of the calculated response from the transient load and the average normalized PSD from the measurements are shown. It was discovered that similarities between the calculation and the measurements existed in the U1-direction for the point Roof and the U3-direction for the point Wall.

To sum up it was noted that the transient load case of a single axle could give a hint about the displacement magnitude which is generated during a passage of a vehicle. However, in order to fully describe the passage in terms of time duration it was concluded that a more refined load-case is needed.

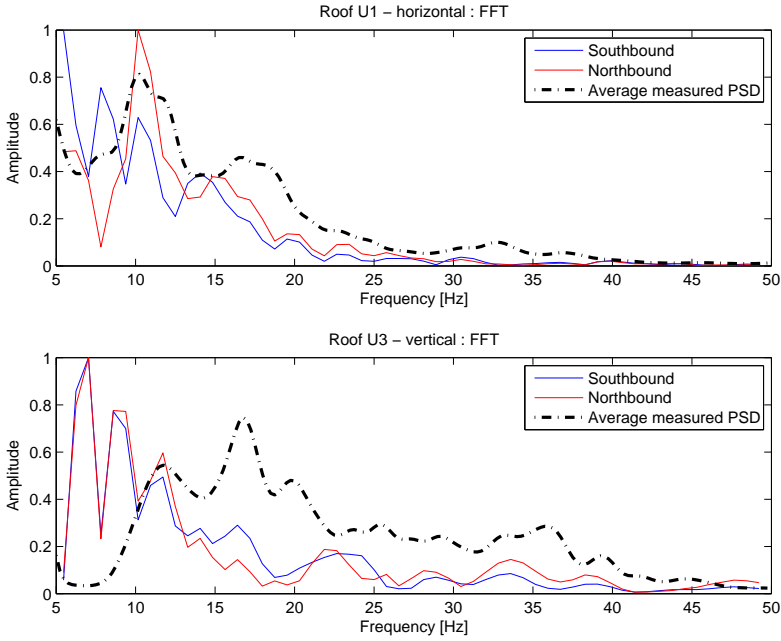


Figure 7.14: Comparison of frequency content from transient response and measurements at position Roof

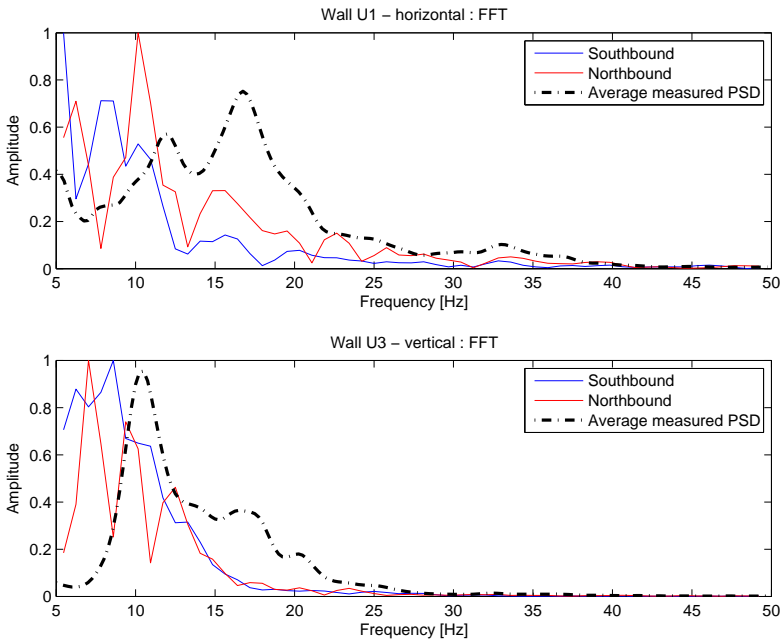


Figure 7.15: Comparison of frequency content from transient response and measurements at position Wall

Chapter 8

Conclusions and suggestions for further work

During the work of this thesis the following main conclusions were made:

- The load case described by the single axle model could be used for an approximation of a vehicle.
- The predicted displacements from the single axle model generated vibration levels below 20 nm (1 s RMS) in all directions. The suggested transient load case could therefore not explain the high level of vibrations (>200 nm 1 s RMS > 5 Hz) which had been measured previously.

One conclusion which also could be made during the study was that a realistic description of the load case was of extremely importance in order to capture the behavior of a road-bridge during passages of vehicles. The measurements indicated that the load case from a vehicle consisted of a complex combination of different exciting frequencies. It is therefore suggested that further work would focus on how to describe a more refined load case. A starting point could be to investigate and determine the real shape profile and the real stiffness of the road thus enabling a more realistic description of the load generating geometry. It would be highly interesting to further analyze the event of a vehicle passage using a fully combined vehicle- road interaction simulation. Such simulation could also be combined with more refined measurements. Further work could also focus on how to set up a more controlled measurement situation, for example to use a standardized vehicle which could be run over the road-bridge multiple times and at various speeds. Possible further experimental studies could also include a controlled force pulse using falling weights and structural shakers. With more controlled experiments it would be much easier to separate the influence from the road and the influence from the road-bridge. Investigations of the data from the seismometer could also probably be useful in the continued study.

Bibliography

- PE Austrell, O. Dahblom, J. Lindemann, A. Olsson, KG Olsson, K. Persson, H. Petersson, M. Ristinmaa, G. Sandberg, and PA Wernberg. *CALFEM: A Finite Element Toolbox: Version 3.4*. Structural Mechanics, LTH, 2004.
- D. Cebon. *Handbook of vehicle-road interaction*. Swets & Zeitlinger, 1999.
- A.K. Chopra. *Dynamics of structures*, volume 1. Prentice Hall, 1995.
- S. Krenk. *Non-linear modelling and analysis of solids and structures*. Cambridge University Press Cambridge, 2009.
- N.S. Ottosen and H. Petersson. *Introduction to the finite element method*. Prentice-Hall, 1992.
- N.S. Ottosen and M. Ristinmaa. *The mechanics of constitutive modeling*. Elsevier Science, 2005.
- O.C. Zienkiewicz and R.L Taylor. *Finite Element Method: Volume 1 - The Basis*. Butterworth-Heinemann, Oxford, 5th edition, 2000.